Earthquake Engineering & Structural Dynamics

WILEY

RESEARCH ARTICLE OPEN ACCESS

An SSI-Informed Design for Tuned Mass Dampers With Small-to-Large Mass Ratios

Davide Noè Gorini[1] | Pasquale Roberto Marrazzo[2] | Elide Nastri[2] | Rosario Montuori[2]

[1]Department of Civil, Environmental and Mechanical Engineering, University of Trento, Trento, Italy | [2]University of Salerno, Fisciano, SA, Italy

Correspondence: Davide Noè Gorini (davidenoe.gorini@unitn.it)

Received: 26 July 2025 | **Revised:** 3 April 2026 | **Accepted:** 5 May 2026

Keywords: dynamic soil-structure interaction | hazard-resistant superelevation | OpenSees | optimum vibration control | TMD

ABSTRACT

Tuned Mass Dampers (TMDs) are used to mitigate structural vibrations induced by seismic or wind excitation, by tuning the device to the system's dominant resonant frequencies. However, the TMD effectiveness can be undermined by soil-structure interaction, which can lead to elongation of the vibration periods and to combined translational-rotational deformation modes. Despite its importance, this interaction is neglected in conventional TMD design. To address this gap, the present study proposes an integrated design methodology for TMDs aimed at minimising earthquake-induced effects in the superstructure, encompassing both conventional and Large Mass ratio TMDs. Optimal TMD configurations are identified through a comprehensive parametric analysis formulated in a rigorous nondimensional framework, in which soil-structure-TMD interaction is simulated by a recently developed, practice-oriented numerical model (SimilSDOF). Optimum TMD parameters are accordingly correlated to factors controlling the overall dynamic response, yielding straightforward design formulas. The proposed SSI-informed design not only avoids the occurrence of detrimental effects caused by soil-structure interaction but also leverages the dynamic response of the foundation system to enhance the TMD performance. The proposed method is validated by means of a two-stage approach: (i) an extensive investigation using the SimilSDOF, and (ii) nonlinear dynamic analyses of continuum-based, coupled soil-building models.

1 | Introduction

By virtue of their conceptual simplicity and potential, Tuned Mass Dampers (TMDs) have garnered notable attention in both research and design domains, leading to substantial advancements over time. In its most elementary form, a TMD consists of a mass connected to the primary structure via a translational linear spring and damper. A foundational design approach was introduced by Den Hartog [1], who derived closed-form expressions for the optimal mass, stiffness and damping ratio of a conventional TMD minimising oscillations of the superstructure. The latter is therein idealised as a single degree of freedom system (SDOF) exhibiting linear elastic behaviour and subjected to harmonic horizontal loading. Albeit such simplifications, Den Hartog's solution remains a benchmark in TMD design, owing to its straightforward nature and rigorous analytical basis. Moreover, although an optimal TMD configuration should ideally account for the variable frequency content of real earthquake ground motion, Den Hartog's criterion was proved to be nearly optimal even in the case of pulse-like excitations and more complex loading scenarios [2, 3].

Subsequent research aimed to investigate the dynamic performance of TMDs more comprehensively, including the influence of damping and the multimodal features of the structural layout [4–7]. Warburton [8] and Sadek et al. [9] derived empirical abacuses to identify optimal TMD properties while accounting for the inherent dissipative contribution of the primary structure, modelled through a linear viscous damper in parallel to the SDOF representation. Further insights have been gained into the sensitivity of TMD performance to structural irregularities, which introduce uncertainty in optimal tuning because of the activation of multiple vibration modes contributing to the dynamic response [5]. This issue can be addressed by using multiple TMDs at strategically selected elevations within the superstructure [10, 11] or adopting semi-active devices [12].

An efficient remedy to improve the TMD performance involves increasing its mass ratio, G_1, intended as the ratio between the TMD mass and that of the superstructure. Conventional devices are characterised by a mass ratio not greater than 5% due to practical limitations, such as the excessive overburden for the primary structure or insufficient space for installation. Nonetheless, it is well known that, compared to conventional devices, greater G_1 values can a) be more efficient in mitigating dynamic effects and b) provide greater robustness in tuning the TMD to the structure's dynamic characteristics [6, 7, 13–15]. To achieve this, some solutions have been explored over the years. These include incorporating an inerter magnifying the stabilising inertial forces developing in the TMD [16–20], or more recently integrating the TMD as a superelevation of the main structural layout. The latter solution is termed Large Mass ratio TMD (LM-TMD) as it enables to attain values of G_1 up to 30%–40%. LM-TMDs also offer a dual benefit as seismic retrofitting solutions of low- to mid-rise existing buildings while simultaneously expanding usable space [7]. De Angelis et al. [13], Yahyai et al. [14] and Marrazzo et al. [15] developed tuning solutions for LM-TMDs based on a simplified two-DOF system (structure + LM-TMD), with reference to linear structures featured by a mono-modal response and neglecting soil-structure interaction [21–23].

Typical design of TMDs overlooks the influence of soil-structure interaction, despite growing evidence that this interaction can significantly reduce or even compromise the TMD effectiveness. Soil-structure interaction can indeed (i) elongate the vibration periods, (ii) couple translational and rotational deformation modes and (iii) magnify irreversible effects in the structural system. Over the past three decades, this has been confirmed through analytical, numerical and experimental studies. With reference to conventional TMDs ($G_1 \leq 5\%$), Wu et al. [24] and Takewaki [25] showed that a coupled dynamic response between soil and structure can diminish the effectiveness of a tuned damper system. Similarly, using a frequency-independent numerical model, Wu et al. [26] further demonstrated that, for a given structural layout, decreasing the soil stiffness reduces the TMD effectiveness. In response, Ghosh and Basu [27] proposed tuning conventional TMDs to the fundamental frequency of the entire soil-structure system, using the optimal solution for a SDOF under harmonic loading [1]. It was an intuitive extension of Den Hartog's criterion but turned out to be effective only for structures exhibiting predominant translational responses, that is, when foundation rocking is negligible [28]. Subsequently other optimisation strategies were developed by Farshidianfar and Soheili [29, 30], Bekdas and Nigdeli [31] and Salvi et al. [32] for conventional TMDs referring to specific layouts including soil-structure interaction.

To foster a more comprehensive understanding of soil-structure-TMD interaction, Gorini and Chisari [28] carried out a global sensitivity analysis using a simplified interpretative model, called SimilSDOF, accounting for the frequency-dependent features and combined translational-rotational deformation modes of the soil-structure layout. It was therein demonstrated that the TMD performance, in addition to the parameters used in standard design [1], is also controlled by the structure-to-soil relative stiffness, the foundation aspect ratio, the structural slenderness and the distribution of mass in the structural layout. Lately, similar considerations were found for LM-TMDs [7] through nonlinear dynamic analyses involving a continuum-based, fully coupled soil-building model equipped with a LM-TMD. It was seen that a sufficiently large mass ratio can partly mitigate the adverse effects of the soil compliance.

In light of this evolving context, the present paper introduces an SSI-informed design criterion for the optimal mechanical properties of conventional and Large Mass ratio TMDs, incorporating the dependence of the TMD performance on key factors relating to soil-structure interaction. This is achieved by elaborating the results of a massive parametric study on dynamic soil-structure-TMD interaction using the SimilSDOF [28], as recounted in Sections 2, 3. In Section 4, optimal TMD configurations are identified and correlated to the dominant non-dimensional parameters of the problem according to multi-dimensional best-fitting techniques. The proposed design approach is finally validated in Section 5.

2 | Computational Framework

2.1 | Interpretative Model

A parametric study was carried out to identify optimal configurations of both conventional and LM-TMDs in soil-building layouts. Time-domain dynamic analyses were performed using the SimilSDOF model [28], chosen for its ability to (i) support a large number of simulations and (ii) standardise the dominant effects associated with linear soil-structure-TMD interaction. The SimilSDOF, schematically illustrated in Figure 1, is composed of a mass m_2 located at the top of the model and connected to a lower mass m_1, positioned at height h_1, through the parallel connection of a translational linear spring and dashpot with stiffness k_s and damping coefficient c_s. A rotational inertia I_{rg} is assigned to mass m_1, which is in turn rigidly linked to the foundation: this configuration enables to account for a barycenter height of the superstructure different from its modal height, as a factor affecting the TMD performance [28].

The foundation has a mass and rotational inertia, m_f and I_f, and is supported by the parallel combination of a linear spring and a dashpot for each horizontal and rotational degree of freedom, reproducing frequency-dependent soil-structure interaction effects in the linear regime. The TMD, with mass m_{TMD}, is attached to m_2 at an elevation h_{TMD} by means of a spring with stiffness k_{TMD} placed in parallel with a dashpot of coefficient c_{TMD}. The TMD mass is constrained to move in the horizontal direction only. The geometric and physical parameters of the SimilSDOF are listed in Table 1.

The comparison with advanced experimental and numerical models [28] demonstrated that the SimilSDOF provides a reliable

TABLE 1 | Geometric and physical quantities of a linear soil-structure-TMD system.

	Number	Symbol	Dimension	Description
structure	1	m_s	M	*mass of the structure*
	2	m_m	M	*modal mass of the structure*
	3	ω_s	1/T	*fundamental circular frequency of the structure*
	4	$c_{\phi s}$	M/T	*damping coefficient of the structure*
	5	h_m	L	*modal height of the structure*
	6	$h_{G,s}$	L	*barycentre height of the structure*
	7	r_g	L	*radius of gyration of the structure*
TMD	8	m_{TMD}	M	*mass of the TMD*
	9	h_{TMD}	L	*height of the TMD*
	10	k_{TMD}	M/T^2	*stiffness of the TMD*
	11	c_{TMD}	M/T	*damping coefficient of the TMD*
soil-foundation	12	ρ_s	M/L^3	*mass density of soil*
	13	V_s	L/T	*shear wave velocity of soil*
	14	ρ_c	M/L^3	*mass density of the foundation*
	15	d_w	L	*depth of the foundation (Z-direction)*
	16	$L_{f,x}$	L	*semi-length of the foundation in the X-direction*
	17	$L_{f,y}$	L	*semi-length of the foundation in the Y-direction*

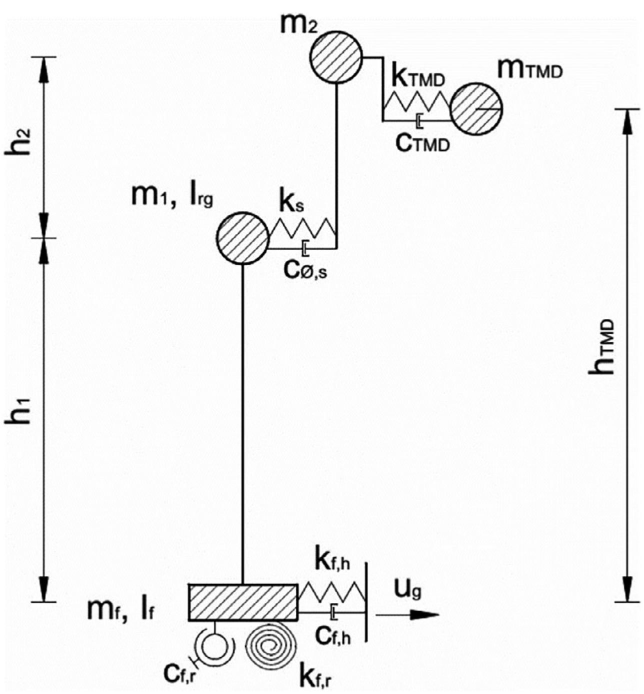

FIGURE 1 | SimilSDOF: Soil-structure-TMD interpretative model (reproduced from 28).

approximation of linear soil-structure-TMD interaction, making it particularly suited for parametric assessments by virtue of its extremely low computational cost. The assumption of linear soil behaviour can be considered appropriate for moderate dynamic excitation or may be interpreted as a linearised approximation of a nonlinear response in secant terms. When significant nonlinear soil behaviour is expected, the stiffness of the soil-foundation system can be estimated either, in first approximation, from small-strain soil properties or, when site-specific free-field seismic response analyses are available, from an operational soil stiffness representative of the expected level of mobilised strength under the design seismic scenarios. Moreover, previous studies [7] showed that the dynamic response of LM-TMDs does not significantly alter the dominant features of soil-foundation interaction. This implies that the conceptual framework of the SimilSDOF, originally developed for conventional TMDs, can be effectively extended to systems with large mass ratio.

In its current form, the SimilSDOF is especially applicable to simulate the dynamic response of planar structures (albeit its extension to the 3D case is straightforward) whose dynamic response is dominated by the fundamental vibration mode. Under these conditions, the physical interpretation of the SimilSDOF parameters is as follows: the total structural mass is equal to $m_s = m_1+m_2$, where m_2 represents the modal mass, and the modal height is $h_m = h_1+h_2$; accordingly, the barycentre height and the radius of gyration of the structure can be written as $h_{G,s} = (m_1h_1+m_2h_m)/m_s$ and $r_g = [(m_1h_1+m_2h_2+I_{rg})/m_s]^{0.5}$, respectively.

The SimilSDOF can be perturbed by translational and/or rotational ground motion to carry out dynamic analyses in the frequency or time domain. In Gorini and Chisari [28], a frequency-domain approach was adopted to point out the dominant parameters influencing the dynamic performance of TMDs. That implementation, carried out in Abaqus [33], was used to carry out steady-state dynamic analyses with frequency-dependent stiffness and viscous coefficients assigned to the elements of the soil-foundation system. In contrast, we use the SimilSDOF in time-domain dynamic simulations within

TABLE 2 | Variability of the non-dimensional groups (dominant groups in bold).

Non-dimensional groups	Definition	Ranges
G_1. TMD mass ratio	$m_{\mathrm{TMD}}/m_{\mathrm{m}}$	0.1–0.4
G_2. TMD frequency ratio	$\omega_{\mathrm{TMD}}/\omega_{\mathrm{s}}$	0.4–2.0
G_3. TMD damping ratio	$c_{\mathrm{TMD}}/2\sqrt{m_{\mathrm{TMD}}\, k_{\mathrm{TMD}}}$	0.15–0.25
G_4. Normalised TMD height	$h_{\mathrm{TMD}}/h_{\mathrm{m}}$	1.5
G_5. Foundation embedment ratio	$d_{\mathrm{w}}/L_{\mathrm{f,x}}$	0.0533
G_6. Structure-to-soil relative stiff.	$h_{\mathrm{m}}/(V_{\mathrm{s}} \cdot T_{\mathrm{s}})$	0.07–0.8
G_7. Slenderness ratio	$h_{\mathrm{m}}/L_{\mathrm{f,x}}$	0.5–2.0
G_8. Soil-structure relative mass	$m_{\mathrm{tot}}/(\rho_{\mathrm{s}} \cdot L_{\mathrm{f,x}}{}^3)$	2.2
G_9. Foundation aspect ratio	$L_{\mathrm{f,x}}/L_{\mathrm{f,y}}$	0.5–1.0
G_{10}. Damping ratio	$c_{\phi\mathrm{s}}/(2\,\omega_{\mathrm{s}}\, m_{\mathrm{m}})$	3%–5 %
G_{11}. Effective mass ratio	$m_{\mathrm{m}}/m_{\mathrm{s}}$	0.736
G_{12}. Normalised rocking height	$(h_{\mathrm{G,s}}m_{\mathrm{s}} - h_{\mathrm{m}}m_{\mathrm{m}})/[(m_{\mathrm{s}} - m_{\mathrm{m}})h_{\mathrm{m}}]$	0.102
G_{13}. Normalised radius of gyration	$h^2_{\mathrm{m}}m_{\mathrm{m}}/(r^2_{\mathrm{G}}m_{\mathrm{s}}) - (h_{\mathrm{G,s}}m_{\mathrm{s}} - h_{\mathrm{m}}m_{\mathrm{m}})^2/[r^2_{\mathrm{G}}m_{\mathrm{s}}(m_{\mathrm{m}} - m_{\mathrm{s}})]$	0.1–0.5
G_{14}. Norm. foundation mass density	$\rho_{\mathrm{c}} \cdot h_{\mathrm{m}}{}^3/m_{\mathrm{m}}$	1.5–25.0

the finite-element analysis framework OpenSees [34], which is selected for its open-source availability and as a stepping stone towards the future extension of the SimilSDOF to the nonlinear soil behaviour. In this context, the spring-dashpot pairs modelling the soil-foundation system must be frequency independent. To compensate, each pair is combined with a mass/rotational inertia ($m_{\mathrm{SSI}}/\mathrm{I}_{\mathrm{SSI}}$) assigned to the foundation node calibrated to reproduce the fundamental vibration modes of the foundation system. These quantities include the mass and rotational inertia of the foundation members and the mass of the soil participating in the dynamic response of the footing, which were identified through existing elastic solutions [35]. Preliminary verifications, omitted for conciseness, confirmed that the Abaqus and OpenSees implementations produce identical results under both harmonic and seismic excitation.

2.2 | Nondimensional Form

The SimilSDOF is susceptible of the rigorous nondimensional description in Table 2, derived through the Buckingham-π theorem. When the response of the soil-foundation system is inhibited, the SimilSDOF degenerates into the classical two-DOF model ($m_2 + m_{\mathrm{TMD}}$) used in standard design criteria. In its full form, however, all nondimensional groups in Table 2 can be varied independently. Through a rigorous, global sensitivity analysis, Gorini and Chisari [28] demonstrated that the TMD performance is governed by a few nondimensional groups only, namely: G_1 to G_3 and G_{10}, which appear in conventional design approaches, G_6, G_7, G_9, G_{13} and G_{14}, which are associated to the interaction of the structure with the surrounding soil. Specifically, G_6 represents the structure-to-soil relative stiffness, serving as a concise indicator of the dynamic coupling between the response of the superstructure and that of the foundation system. Groups G_7, G_9, G_{13} and G_{14} characterise the distribution of mass in the structural layout, which governs foundation rocking, with G_{13} expressing the ratio between the second moment of mass of the lumped masses and the total rotational inertia. These dominant groups are adopted as reference parameters in the identification of optimal TMD configurations (see Section 4).

3 | Numerical Workflow

The nondimensional form in Section 2 underpins the computational workflow used to investigate optimal TMD configurations. A broad parametric study was carried out using the SimilSDOF varying the dominant non-dimensional groups according to the ranges listed in Table 2, to represent a range of soil-structure layouts relevant to civil engineering practice.

The TMD mass ratio was varied in a wide range, considering both conventional devices to LM-TMDs (G_1>5%). The variability of the TMD frequency ratio G_2 was calibrated to ensure the exploration of configurations that maximise vibration mitigation, while the TMD damping ratio G_3 was selected to reflect the dissipative properties of dampers commonly used in practice. According to the performance regions identified by Gorini and Chisari [28], G_6 spans from values representing negligible soil-structure interaction ($G_6 \leq 0.08$) to configurations in which the dynamic response of the structure is dominated by the soil compliance (G_6> 0.6); in the intermediate region (0.08< G_6< 0.6) the dynamic response of the superstructure is significantly coupled to that of the soil-foundation system. The range assumed for G_7 involves low-to-medium slender structures, that are realistic targets for the implementation of LM-TMDs, as discussed in Section 1. Group G_9 represents the aspect ratio of the entire foundation system. Therefore, the assumed range for G_9 encompasses square- or rectangular-shaped footprints of the building, with a minimum ratio between the plan dimensions of 0.5. The structural damping ratio was set to values representative of the behaviour in the linear regime, given that the TMD's purpose is to prevent significant nonlinear responses under dynamic excitation. Groups G_{13} and G_{14} varied within ranges known to significantly affect the TMD performance, as reported by Gorini and Chisari [28]. The remaining, non-dominant groups have a marginal effect on the TMD performance [28], hence they were kept constant in the parametric study and were defined based on the characteristics of the eight-storey reinforced-concrete building equipped with a LM-TMD extensively analysed in Gorini et al. [7] (the latter will be described in Section 5.2.1, devoted to the method's validation).

All permutations of the selected values for the non-dimensional groups were investigated, resulting in a total of 373'248 soil-structure-TMD cases. For each case, a sequence of harmonic displacement time histories with unit amplitude was applied to the base of the SimilSDOF, covering 31 values of the external

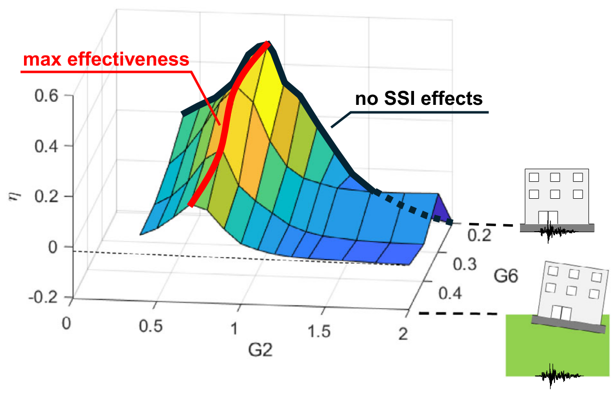

FIGURE 2 | TMD effectiveness, η, plotted as a function of the TMD frequency ratio, G_2, and the structure-to-soil relative stiffness, G_6.

excitation period within the range (0.1-4)×T_1, where $T_1 = 2\pi(m_2/k_s)^{0.5}$ is the fundamental vibration period of the superstructure. The adopted frequency bandwidth encompasses the range of interest for the dynamic amplification of each soil-structure-TMD system. Each configuration was also analysed without the TMD to establish a benchmark for assessing its effectiveness.

The TMD effectiveness is quantified in terms of its ability to reduce the deformations in the superstructure. Therefore, the effectiveness for the i^{th} soil-structure layout is defined as:

$$\eta_{\mathrm{i}} = \frac{\max\left\{u_{\mathrm{i}}^{(\mathrm{NoTMD})}\right\} - \max\left\{u_{\mathrm{i}}^{(\mathrm{TMD})}\right\}}{\max\left\{u_{\mathrm{i}}^{(\mathrm{NoTMD})}\right\}} \tag{1}$$

where max{$u_i^{(\mathrm{NoTMD/TMD})}$} denotes, for the i^{th} soil-structure system, the maximum deformation of the spring with stiffness k_s (see Figure 1), representing in the SimilSDOF context the overall deformability of the superstructure, varying the period of the ground motion.

4 | Design Correlations

This study aims to enhance the TMD performance by achieving a convenient balance between the frequency and dissipative features of the soil-structure system. In line with standard practice, G_1 is treated as design input, typically constrained by construction requirements. Accordingly, G_2 and G_3 are identified as the target quantities to be optimised. To pursue this objective, the results from the extensive study presented in Section 3 were processed to determine the optimum pair G_2-G_3 maximising the TMD effectiveness for each soil-structure layout and TMD mass ratio.

4.1 | TMD Frequency Ratio

An initial insight into the results of the parametric study is provided in Figure 2, which relates the TMD effectiveness η to the structure-to-soil relative stiffness, G_6, and the TMD tuning factor, G_2. For clarity, the representation focuses on a subset of results, namely, $G_1 = 0.2$, $G_3 = 0.2$, $G_7 = 1.0$, $G_9 = 1.0$, $G_{10} = 0.03$, $G_{13} = 0.1$. It is evident that the TMD effectiveness increases significantly under negligible soil-structure interaction effects (G_6<0.2, *no SSI effects* locus in the figure). In particular, the effectiveness becomes maximum for $G_2 = 0.85$, which aligns with the value prescribed by classical analytical solutions for a SDOF system with no soil-structure interaction effects [1]. For other values of G_2, the TMD is no longer optimally tuned to the dynamic response of the superstructure, resulting in a reduced effectiveness. The latter assumes even negative values (i.e., the TMD amplifies structural vibration) for sufficiently large G_2.

Soil-structure interaction alters radically the TMD's optimal performance. Indeed, the maximum effectiveness η_{OPT} reduces remarkably as the structure-to-soil relative stiffness rises: η_{OPT} decreases from 0.5, for G_6<0.2, to 0.18 when $G_6 = 0.6$. Specifically, the TMD performance deteriorates rapidly in the range $G_6 = 0.2$-0.5, for then stabilising for larger G_6. This trend is consistent with the preliminary performance regions found in Gorini and Chisari [28], where it was observed that $G_6 \geq 0.5$ corresponds to systems in which the soil compliance dominates the overall dynamic response. Moreover, the *max effectiveness line* in Figure 2 shows a distinct relationship between the optimum tuning factor $G_{2,\mathrm{OPT}}$ and the structure-to-soil relative stiffness. As G_6 increases, the optimal tuning factor shifts to lower G_2, stabilising at $G_2 = 1.2$ for $G_6 \geq 0.5$. This shift can be ascribed to the fact that the more the soil compliance compared to the superstructure deformability, the lower the natural frequency of the soil-structure system, which requires in turn a lower vibration frequency of the TMD to achieve optimal tuning. For $G_6 \geq 0.5$, improper tuning can even lead to detrimental effects caused by the TMD (η<0) driven by the emergence of coupled translational-rotational deformation modes of the soil-foundation system. Notwithstanding, even under these adverse conditions, proper tuning of the TMD can still ensure effective vibration control.

The results above underscore the existence of optimal tuning regimes for TMDs that leverage the dynamic coupling among soil, foundation, superstructure and device. However, optimal tuning is also influenced by the remaining dominant parameters. For instance, Figure 3 examines, for each TMD mass ratio, the variability of $G_{2,\mathrm{OPT}}$ with G_6 and as a function of another crucial parameter, the structural slenderness G_7, referring to $G_3 = 0.2$, $G_9 = 1.0$, $G_{10} = 0.03$ and $G_{13} = 0.1$ for clarity. Interestingly, $G_{2,\mathrm{OPT}}$ exhibits a Gaussian-like dependence on G_6 and G_7, with an evident peak at large structure-to-soil relative stiffness. In detail, for a low deformability of the foundation system compared to that of the superstructure ($G_6 \leq 0.2$), $G_{2,\mathrm{OPT}}$ slightly depends on the structural slenderness as the latter marginally impacts the deformation mode of the superstructure that remains predominantly translational. As G_6 rises, G_7 becomes more influential, with a maximum of $G_{2,\mathrm{OPT}}$ attained for $G_7 = 1$ regardless the TMD mass ratio. The peak of $G_{2,\mathrm{OPT}}$ corresponds to cases in which the structural slenderness is sufficiently high to couple dynamically the translational and rotational response of the soil-foundation system, requiring a larger tuning frequency of the TMD compared to the one of the superstructure. For greater G_7 values, the rocking mode at the foundation level, exalted by the concomitant presence of a large G_6, becomes predominant compared to translational modes, implying much lower frequency ratios of the TMD to achieve effective vibration suppression. Similar considerations hold for cases with different foundation aspect ratios, G_9; the relative results are provided in Appendix A.

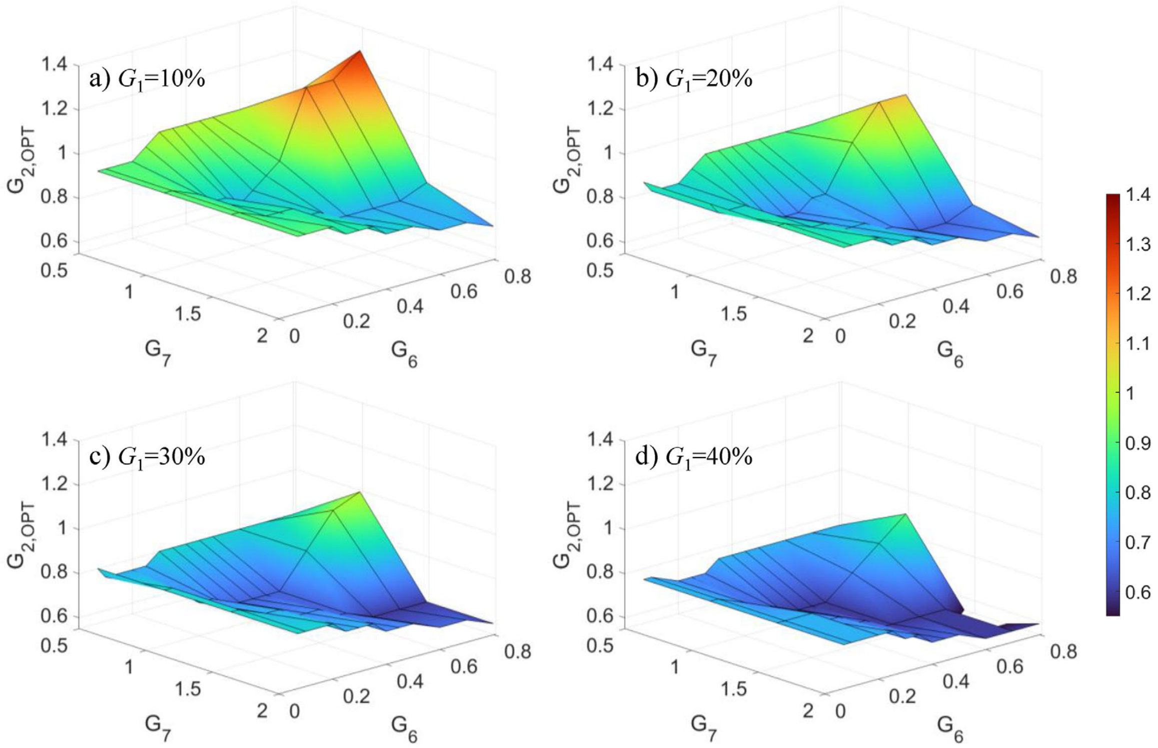

FIGURE 3 | Optimum values of the TMD frequency ratio, $G_{2,\mathrm{opt}}$, plotted as a function of the structure-to-soil relative stiffness, G_6, and the structure slenderness ratio, G_7, for TMD mass ratios $G_1 = 10, 20, 30, 40\%$ (a, b, c and d, respectively), for $G_9 = 1$.

These considerations hold across the full space of the non-dimensional parameters analysed in the present study. Nevertheless, the use of a TMD Mass Ratio $G_1 = 0.3$–0.4 (Figs. 3c,d) enhances the effectiveness and reduces the sensitivity of optimal tuning to variations in both G_6 and G_7. In these cases, $G_{2,\mathrm{OPT}}$ remains within a narrower range, 0.7–1.0, as an indicator of the higher robustness of LM-TMDs compared to conventional TMDs. It is also worth noting that, in all cases, the optimal tuning values derived from this study differ remarkably from those given by conventional design approaches: according to Den Hartog's criterion [1], G_2 falls within the range 0.72–0.91 for the structural layouts considered in the parametric study. The implications of these deviations on the overall dynamic performance will be discussed in Section 5.

4.1.1 | Analytical Form for Optimal Tuning of TMDs

Building upon the results presented in Section 4.1, this section aims to establish a correlation between the optimum TMD tuning factor and the dominant non-dimensional groups characterising the soil-structure layout, that is, $G_{2,\mathrm{OPT}} = \hat{G}_{2,\mathrm{OPT}}\{G_1, G_6, G_7, G_9, G_{10}, G_{13}, G_{14}\}$. This design criterion was derived by developing a multidimensional best-fitting algorithm, implemented in Matlab [36]. The algorithm performs a global search over a set of C^1 candidate functions of various typology (continuous functions with continuous first derivatives) to identify the one that best fits the full dataset of numerical results. For each candidate, the algorithm computes the optimal coefficients by minimising fitting errors. The goodness of fitting is quantified through widely used statistical indicators, namely: the Coefficient of Determination, R^2, Sum of Squares Error, SSE, Root Mean Square Error, RMSE, and Average Absolute Error, AAE. The goal of the fitting process was to maximise R^2 and minimise RMSE, where values of 1 and 0 respectively correspond to a perfect match between predicted and computed data.

As a result of the fitting procedure, the following analytical expression for the optimal tuning factor is proposed:

$$G_{2,OPT} = \frac{\omega_{\mathrm{TMD}}}{\omega_{\mathrm{s}}} = A + B \cdot G_6 + C \cdot G_7 + D \cdot e^{-\left[\frac{(G_7-1)^2}{0.1} + \frac{(G_6-0.8)^2}{0.05}\right]} + E \cdot G_7 \cdot G_6 + F \cdot G_7 \cdot G_6^3 + H \cdot G_6 \cdot G_7^2 + L \cdot G_6 \cdot G_7^3 + M \cdot G_{10} + N \cdot G_{14} \quad (2)$$

from which the optimum circular frequency of the TMD, ω_{TMD}, can be derived. Equation 2 represents a composite surface: it is characterised by a Gaussian bell in the G_6-G_7 domain modulated with polynomial terms. This structure captures the distinct features of optimal tuning discussed in Figure 3. Moreover, the influence of the remaining relevant parameters, G_1, G_9, G_{10}, G_{13} and G_{14}, is embedded through the parametric dependence of coefficients $I = \{A, B, C, D, E, F, G, H, I, L, M, N\}$, enclosed into Equation 2, via the following polynomial function:

$$I = C_{\mathrm{i},1} + C_{\mathrm{i},2}G_1 + C_{\mathrm{i},3}G_9 + C_{\mathrm{i},4}G_1^2 + C_{\mathrm{i},5}G_1G_9 + C_{\mathrm{i},6}G_9^2 + C_{\mathrm{i},7}G_1^3 + C_{\mathrm{i},8}G_1^2G_9 + C_{\mathrm{i},9}G_1G_9^2 + C_{\mathrm{i},10}G_{13} + C_{\mathrm{i},11}G_{13}G_1 + C_{\mathrm{i},12}G_{13}G_9 + C_{\mathrm{i},13}G_{13}^2G_1 + C_{\mathrm{i},14}G_{13}^2G_9 \quad (3)$$

TABLE 3 | Coefficients of the interpolating functions of $G_{2,\mathrm{OPT}}$ (see Equation 3).

	A	B	C	D	E	F	H	L	M	N
C1	1.1259	−0.6609	−0.1078	−0.0317	1.5137	−0.5190	−0.7641	0.1632	−1.6117	0.0008
C2	−2.3505	2.4507	0.8885	−0.5089	−3.1764	2.8399	−1.6106	0.7971	14.9446	0
C3	−0.0905	1.4543	0.1690	0.2208	−3.9257	1.2604	2.4050	−0.5817	0	−0.0016
C4	6.8974	−11.9612	−2.4874	1.3656	9.2049	−2.8662	6.4819	−3.3646	−64.0894	0
C5	−0.1048	−0.5826	−0.1994	0.2625	0.4377	−4.5418	2.2948	−0.6827	0	0
C6	0.0686	−0.4969	−0.1149	0.1340	1.6208	−0.6370	−1.0660	0.2697	0	0.0010
C7	−7.9296	24.0431	2.6373	0.1675	−37.8991	0.8740	15.5187	−1.6679	81.0158	0
C8	−0.0042	−8.9962	−0.0226	−2.0545	32.2727	2.0230	−28.7566	7.2449	0	0
C9	0.0370	2.9082	0.1563	0.2409	−9.9105	1.9324	7.2177	−1.7075	0	0
C10	0.0345	0.0143	−0.0324	0.0473	−0.1189	−0.0056	0.0717	0.0017	0	−0.0004
C11	0.1360	−0.4637	−0.3390	−0.0652	1.7049	−1.5229	−0.1515	0.0262	0	0
C12	−0.1581	0.7578	0.2379	0.0180	−2.1185	0.1713	1.6203	−0.4563	0	−0.0001
C13	−0.1769	0.2881	0.4226	0.0032	−1.2405	2.1139	−0.6027	0.1459	0	0
C14	0.2388	−1.0677	−0.3805	−0.1070	2.9999	−0.5563	−1.8667	0.5111	0	−0.0005

TABLE 4 | Statistical indicators of the goodness of the analytical solution for $G_{2,\mathrm{opt}}$ with respect to the totality of the numerical results.

$\mathbf{R^2}$	0.7473
MSE	0.0066
RMSE	0.0814
AAE	0.0313

where the optimum values of the coefficients $C_{i,j}$ are listed in Table 3. As an example, Figure 4 shows the flexibility of the polynomials in Equation 3 in capturing the peculiar trends associated with the variability of G_1. Notably, although the number of coefficients is relatively high, they describe a compact nondimensional optimal surface (Equations 2 and 3). In fact, the sufficiency and independence of the selected non-dimensional groups were proved in Gorini and Chisari [28]; then, the dominant groups most affecting the TMD performance were therein identified through rigorous statistical methods [37]. Therefore, under the simplifying assumptions of the considered modelling framework (Section 2.1), the proposed formulation enables direct computation of the optimal tuning factor for both conventional and non-conventional TMDs, based solely on a set of key nondimensional parameters.

The goodness of the best-fitting solution is quantified in Table 4, in terms of the statistical indicators introduced at the beginning of this section. Considering the challenge of fitting a dataset of 373’248 samples in the seven-dimensional space of the dominant parameters, the proposed analytical solution for the optimal TMD frequency demonstrates commendable accuracy. In this regard, Figure 5 compares the analytical solution to the numerical results across the same cases presented in Figure 3. The analytical surface follows well the general trend of optimal tuning in the entire range of TMD mass ratios G_1 = 10%–40%. Considering the whole dataset, the maximum local deviation is equal to 16% for G_1 = 10%, whereas the discrepancies remain below 6% for G_1>10%. Analogous comparisons for G_9 = 0.5–0.75 are illustrated in Appendix A.

4.2 | TMD Damping Ratio

In addition to optimal tuning, it is well known that an enhanced performance of the TMD can be achieved by appropriately balancing its dissipative characteristics. Accordingly, this section focuses on identifying values of the damping ratio G_3 that correspond to the optimal TMD performances discussed in Section 4.1.

To this end, the analysis of the full dataset produced by the parametric study revealed a key distinction between TMDs with a mass ratio G_1 = 10% (the lower bound considered in this study) and those with larger mass ratios. Figure 6 illustrates the effectiveness ratios of TMDs having different G_3. Specifically, Figures 6a,c present the effectiveness ratio between the cases with G_3 = 15% and 20%, plotted against the structure-to-soil relative stiffness G_6 and the structure slenderness G_7, for TMD mass ratios ranging from 20% to 40%. Complementarily, Figures 6b,d show the effectiveness ratio between cases with G_3 = 25% and 20%. The results indicate that increasing the TMD damping ratio generally leads to improved system’s performance. This trend holds in the vast majority of cases (98.9%), with only a small subset (1.1%), consisting of squat structures resting on highly compliant soil compared to the structural deformability (effectiveness ratios lower than unity in Fig. 6b). In these exceptional configurations, a performance saturation effect is observed: when the mass ratio is equal or lower than 20%, the high soil deformability dominates the system response, limiting further gains in TMD effectiveness. However, even in these cases, the maximum reduction in effectiveness ratio remains below 4%, confirming that the phenomenon is both marginal and bounded.

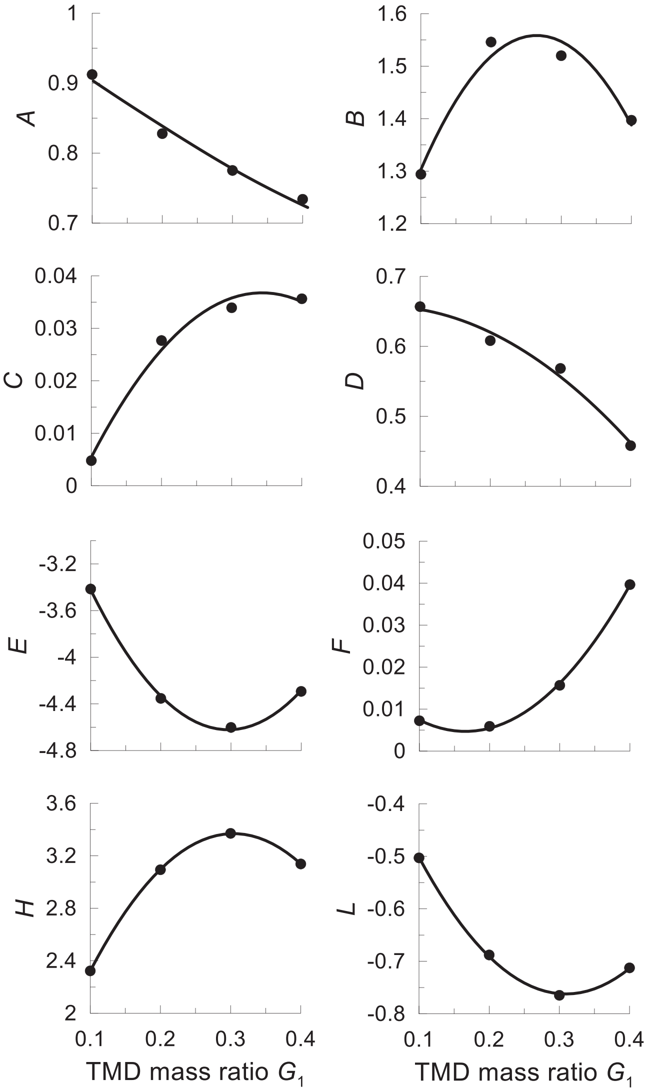

FIGURE 4 | Representation of the interpolating functions {A, B, C, D, E, F, H, L} (continuous lines) for $G_{2,\mathrm{opt}}$ as a function of the TMD Mass Ratio (the dots represent the numerical results).

TABLE 5 | Percentage of soil-structure cases for which the optimum TMD damping ratio, $G_{3,\mathrm{OPT}}$, is equal to 15, 20, 25%, varying the mass ratio.

	% of cases		
G_1	$G_{3,\mathrm{opt}} = 15\%$	$G_{3,\mathrm{opt}} = 20\%$	$G_{3,\mathrm{opt}} = 25\%$
10%	28.2	47.4	24.4
20%	0.2	7.4	92.4
30%	0.0	1.2	98.8
40%	0.0	0.0	100.0

Overall, Table 5 reports the distribution of the optimal TMD damping ratio as a function of the mass ratio. When $G_1 = 10\%$, the influence of damping on the TMD effectiveness appears much more scattered. Indeed, in nearly half of the soil-structure configurations the optimum damping of the TMD is $G_{3,\mathrm{opt}} = 20\%$, whilst the remaining cases are almost evenly split between $G_{3,\mathrm{opt}}$ of 15% and 25%. Nonetheless, design-oriented insights can be still drawn from Figure 7a which, across all soil-structure systems equipped with a 10%-Mass Ratio TMD, shows the average ratios between the effectiveness achieved using only the optimal tuning factor $G_{2,\mathrm{opt}}$ (with a random G_3 between 15–25%), and that obtained considering both $G_{2,\mathrm{opt}}$ and $G_{3,\mathrm{opt}}$. Notably, relying solely on optimal tuning leads to a very slight reduction in effectiveness, no more than 5%.

However, the TMD damping ratio becomes more critical for sufficiently slender structures with very high structure-to-soil relative stiffness, corresponding to the combination $G_6 > 0.6$ and $G_7 \geq 1.5$. In such cases, the dynamic response of the superstructure is strongly affected by coupled translational-rocking modes at the foundation level, which weakens the ability of the TMD to attenuate seismic-induced shear forces in the superstructure: the dynamic coupling between the 10%-Mass Ratio TMD and the superstructure is precarious and the TMD's damping characteristics assume a more relevant role. This is confirmed by Figure 7b, which shows the average effectiveness η (still intended as the mean over cases having $G_1 = 10\%$) associated with the optimised TMD. It can be noticed that, in the critical region discussed above ($G_6 > 0.6$, $G_7 \geq 1.5$), the TMD exhibits the lowest performance, with η dropping to around 10%.

Based on the above findings, the TMD damping ratio is not explicitly optimised to avoid unnecessary design complexities. Nevertheless, the following practical indications can be drawn: when a TMD mass ratio greater than 10% is feasible, the highest level of seismic protection is achieved by combining the optimum tuning factor with the maximum TMD damping ratio available from commercially produced dashpots. Conversely, for TMDs with a mass ratio of 10% or lower, the TMD damping ratio can, as a fist approximation, be selected using existing optimum solutions developed for conventional low-mass ratio TMDs. Hence, unlike the tuning frequency, the optimum damping ratio does not exhibit a sufficiently regular and physically robust dependence on the dominant non-dimensional parameters to justify a dedicated closed-form fitting law over the whole design space. For this reason, the manuscript intentionally provides design-oriented selection criteria for damping, directly inferred from the numerical evidence, rather than introducing an artificial quantitative expression of limited practical and physical significance.

From an operational viewpoint, the SSI-informed design can be implemented in a simple spreadsheet, for immediate use in engineering practice, through the following sequence: (i) evaluation of the dominant non-dimensional groups of the soil-structure system; (ii) determination of the optimal TMD frequency ratio through Equations 2, 3, using the polynomial coefficients reported in Table 3 independently of the specific SSI system under consideration, by virtue of the Buckingham-based non-dimensional formulation; (iii) selection of the damping ratio according to the criteria discussed above.

5 | Validation

The SSI-informed design criterion described in Section 4 is tested through a two-step process. First, its capability to achieve optimal TMD performance is verified using the SimilSDOF. Subsequently, the effectiveness of the optimised design, applied to both

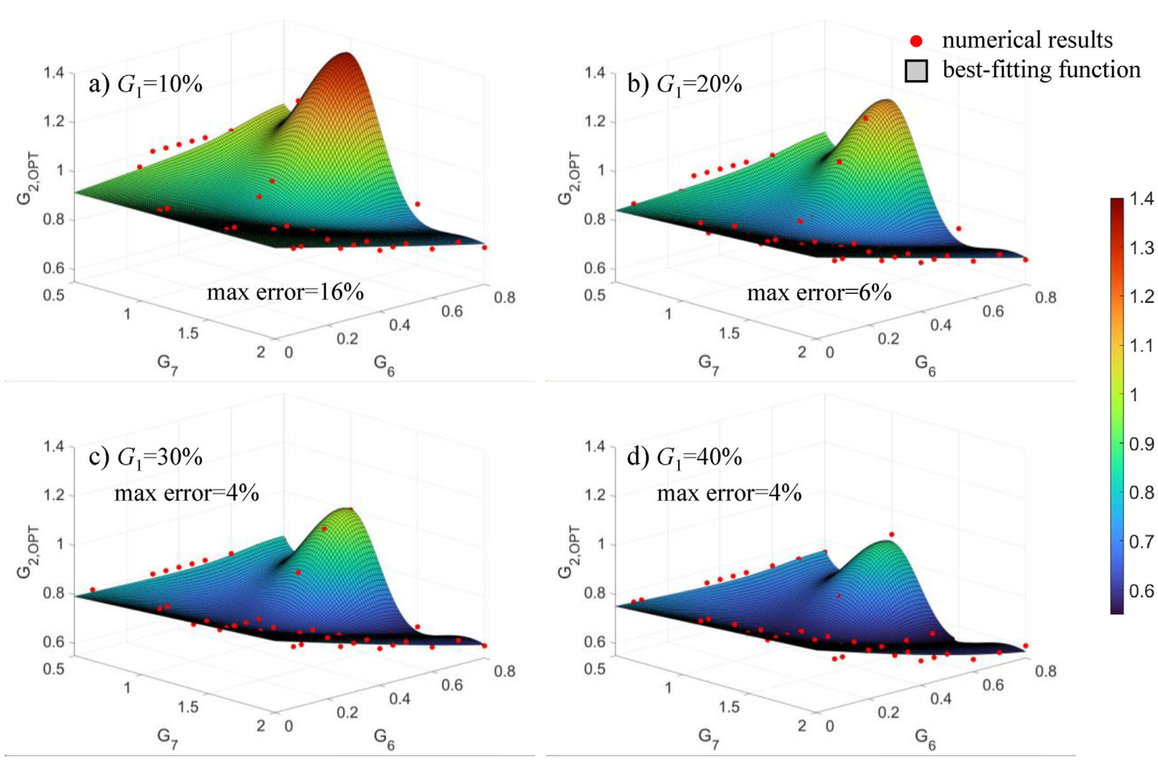

FIGURE 5 | Best-fitting function (surfaces) for the optimum TMD tuning factor, $G_{2,opt}$, versus the SimilSDOF numerical results (dots), plotted as a function of the structure-to-soil relative stiffness, G_6, and the structure slenderness ratio, G_7, for TMD mass ratios $G_1 = 10\%–40\%$, for $G_9 = 1$.

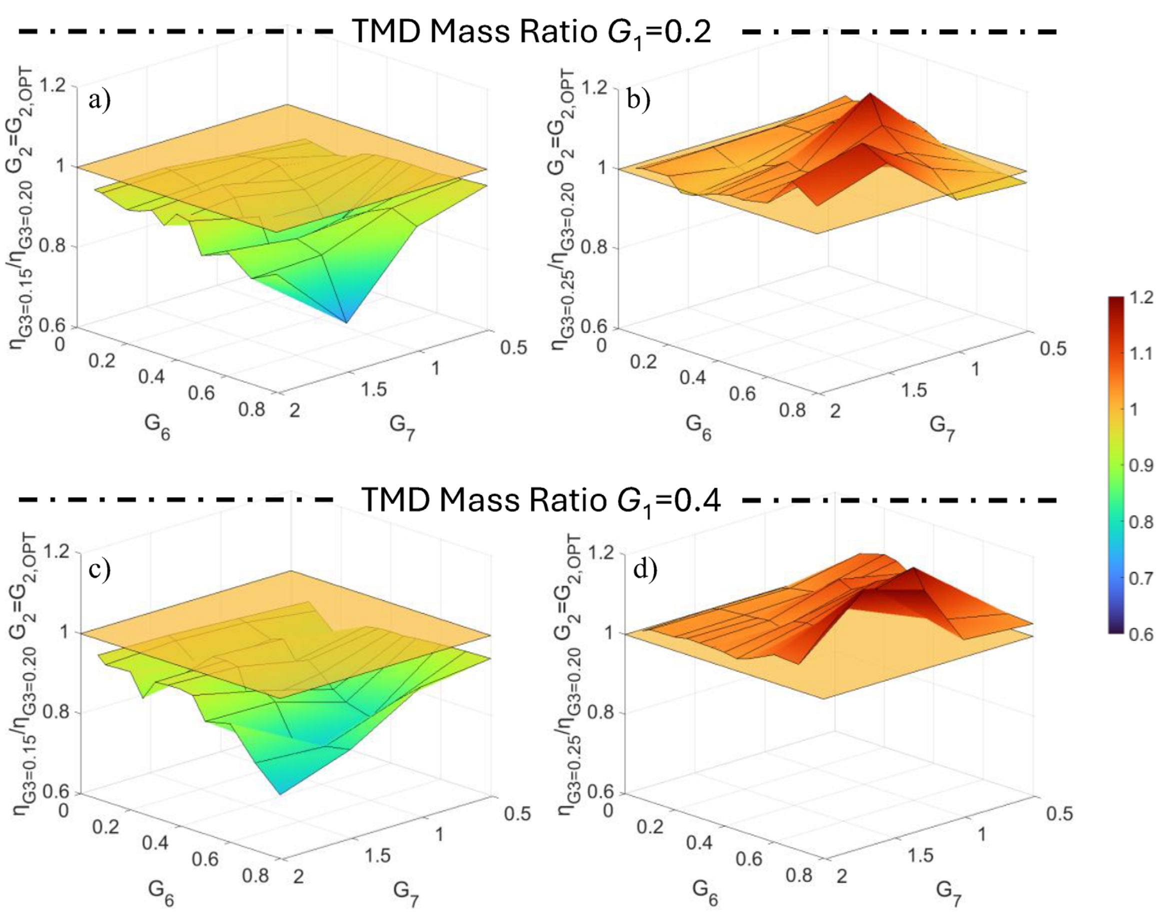

FIGURE 6 | TMD effectiveness ratio (a, c) between cases with TMD damping ratios $G_3 = 0.2$ and 0.15, and (b, d) between cases with $G_3 = 0.25$ and 0.2, plotted as a function of the structure-to-soil relative stiffness, G_6, and the structure slenderness ratio, G_7, for TMD mass ratios of 20%–40%.

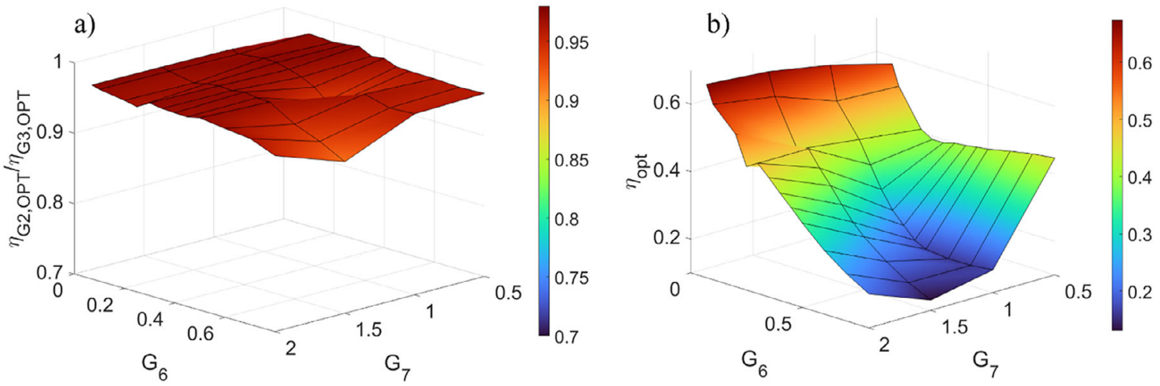

FIGURE 7 | (a) 10%-Mass ratio TMD effectiveness ratio between cases using $G_{2,\text{opt}}$ and those using both using $G_{2,\text{opt}}$ and using $G_{3,\text{opt}}$, plotted as a function of the structure-to-soil relative stiffness, G_6, and the structure slenderness ratio, G_7; (b) optimum effectiveness of a 10%-Mass ratio TMD as a function of G_6 and G_7.

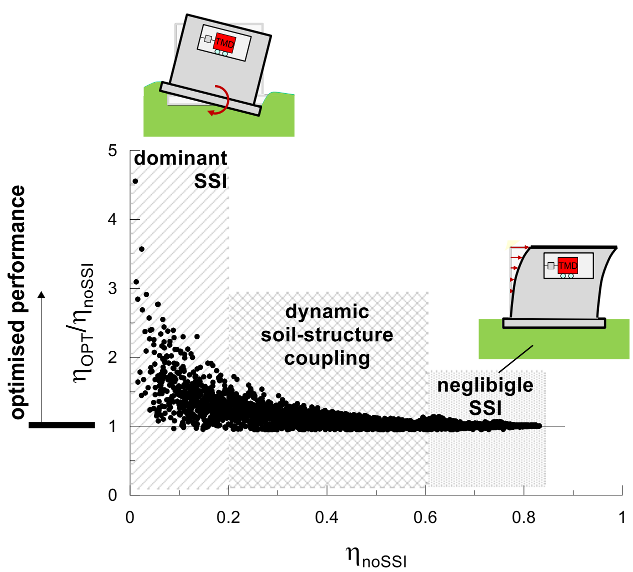

FIGURE 8 | Ratio between the TMD effectiveness obtained with the optimised SSI-informed criterion and the one relating to standard design plotted as a function of the latter for all cases analysed.

conventional and large mass ratio TMDs, is validated with reference to a benchmark case study, analysed via advanced numerical modelling techniques. The beneficial management of SSI is quantified herein not by comparing fixed-base and compliant-base structures in isolation, but by comparing the effectiveness of TMDs designed neglecting SSI with that of TMDs tuned according to the proposed SSI-informed criterion for the same soil-structure system; this directly measures the gain associated with exploiting, rather than ignoring, the coupled soil-structure dynamics.

5.1 | Verification Using the SimilSDOF Model

For the complete set of soil-structure layouts analysed with the SimilSDOF (see Section 3), Figure 8 depicts the ratio between the TMD effectiveness η_{OPT} obtained with the proposed SSI-informed criterion and the effectiveness η_{noSSI} achieved from the conventional design method by Marrazzo et al. [15], that is an extension of the well-known Den Hartog's criterion [1] to TMDs with large mass ratio as well; the data are plotted as a function of η_{noSSI}. Both designed approaches were tested over a broad range of TMD mass ratios, $G_1 = 5\%–30\%$. Hence, to test the effectiveness of the optimised criterion, this verification phase explores a different interval for G_1 from that taken as a reference to derive the SSI-informed criterion ($G_1 = 10\%–40\%$).

Three regions can be identified, corresponding to (i) negligible soil-structure interaction, (ii) significant coupling between the dynamic responses of the structure and of the foundation system, and (iii) response dominated by the large compliance of the foundation soil. In Region (i), conventional design remains nearly optimal, and the SSI-informed criterion naturally converges to it, as desired. However, as the dynamic coupling between the structure and the foundation system intensifies (Region (ii)), the conventional design suffers a marked decline in performance; in contrast, the optimised design maintains superior effectiveness. In Region (iii), the conventional design becomes nearly ineffective. This is due to the highly deformability of the foundation soil relative to the superstructure, which leads to a substantial elongation of the system's vibration periods and magnifies foundation rocking. As a result, a TMD tuned under conventional assumptions, fails to effectively engage with the coupled modes of vibration and can even have detrimental impact on the overall performance ($\eta_{\text{noSSI}}<0$). By contrast, the SSI-informed design significantly enhances the performance by adapting to the coupled translational and rocking modes of the system.

In the 8% of cases, the SSI-informed design results in a slight reduction in effectiveness compared to the conventional approach, with a maximum drop of 5%. To better interpret these marginal cases, Figure 9a shows the variation of $\eta_{\text{OPT}}/\eta_{\text{noSSI}}$ as a function of the structure-to-soil relative stiffness G_6, across the full spectrum of configurations. The figure confirms that traditional TMD tuning becomes increasingly inadequate with growing soil-structure interaction relevance, whereas the proposed approach maintains or even improves performance as G_6 rises.

The cases in which $0.95<\eta_{\text{OPT}}/\eta_{\text{noSSI}}<1$ are distributed rather uniformly across G_6, as it can be observed in Figure 9b. Moreover,

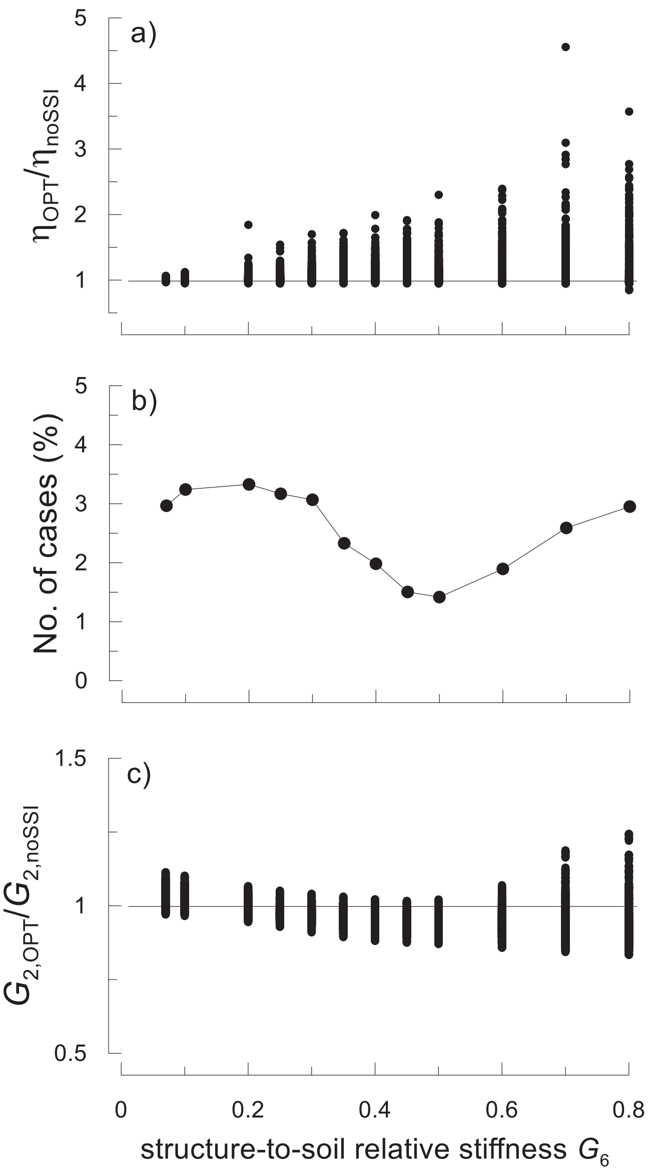

FIGURE 9 | Variability with G_6 of (a) the ratio between the TMD effectiveness obtained with the optimised SSI-informed criterion η_{OPT} and that relating to standard design η_{noSSI}; (b) the aliquot of cases for which η_{OPT}/η_{noSSI} <0; (c) the ratio of the optimised TMD frequency ratio $G_{2,OPT}$ and that predicted by the conventional design $G_{2,noSSI}$.

Figure 9a highlights that the variability of η_{OPT}/η_{noSSI} magnifies with G_6 producing substantial scattering of the data. This result underscores the complex dependence of the TMD effectiveness on all dominant parameters of the problem (see Section 4). Accordingly, Figure 9c illustrates that the optimum tuning factor $G_{2,OPT}$ often diverges significantly from the value $G_{2,noSSI}$ provided by conventional design, with discrepancies reaching up to 25%. The extent of this deviation tends to increase with the prominence of the dynamic coupling between the responses of the superstructure and of the soil-foundation system, reaffirming the inadequacy of no SSI-based tuning rules.

The results discussed above constitute a compelling preliminary validation of the proposed design framework. They demonstrate the potential of the SSI-informed criterion to enhance the tuning

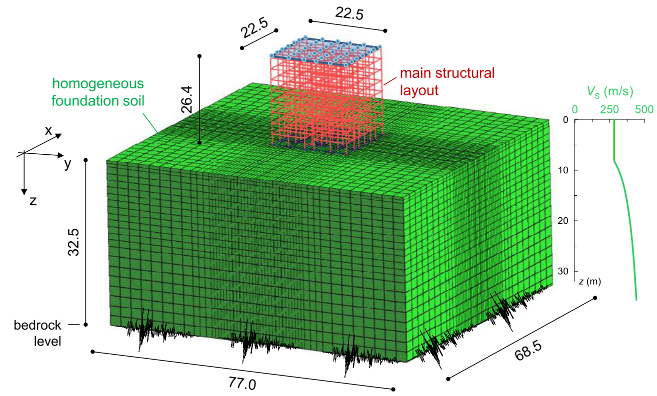

FIGURE 10 | Soil-structure-TMD model implemented in openSees (lengths in meters) and illustration of the profile of the shear wave velocity of soil, V_s, with depth (reproduced from Gorini et al. [7]).

of TMDs in the presence of complex soil-structure dynamics, thereby improving structural safety and serviceability.

5.2 | Validation Using High-Fidelity Modelling

5.2.1 | Case Study

The SSI-informed approach is now validated with reference to a well-documented case study, detailed in Gorini et al. [7]. For brevity, only the essential features of the model are summarised below, whilst the reader can refer to Gorini et al. [7] for an in-depth account of the design process of the structural system and the associated numerical modelling. The benchmark case was simulated through a coupled, continuum-based 3D soil-structure-TMD finite element model, developed in OpenSees and illustrated in Figure 10. The model comprises a total of 55'627 finite elements, of which 53'552 are solid elements modelling the soil domain, while 1'221 and 854 elements model the superstructure and the shallow foundations, respectively. A staged construction analysis was performed to realistically capture the evolution of the stress state within the soil prior to seismic action.

The structural layout is composed of an eight-storey reinforced concrete (RC) building located in the earthquake-prone region of the Messina Strait (southern Italy). The structure is representative of Italian RC buildings from the 1970s and was designed in accordance with technical provisions in force at that time [38], which does not provide specific requirements concerning seismic loading, that is, the building was designed to withstand vertical loads only. The building is characterised by a double symmetry in plan with longitudinal and transverse dimensions of 22.5 m and 24.5 m, respectively, and inter-story height of 3.3 m. In the numerical model, columns and beams are modelled as nonlinear fibre-section beam elements [39, 40]. Each column is supported by an RC shallow foundation connected to the adjacent ones through linking beams. To adequately capture stress concentrations near the foundations, a locally refined mesh was adopted for the surrounding soil.

The soil domain is inspired by the subsoil conditions of the Messina region [41, 42]: it is a dry coarse-grained deposit,

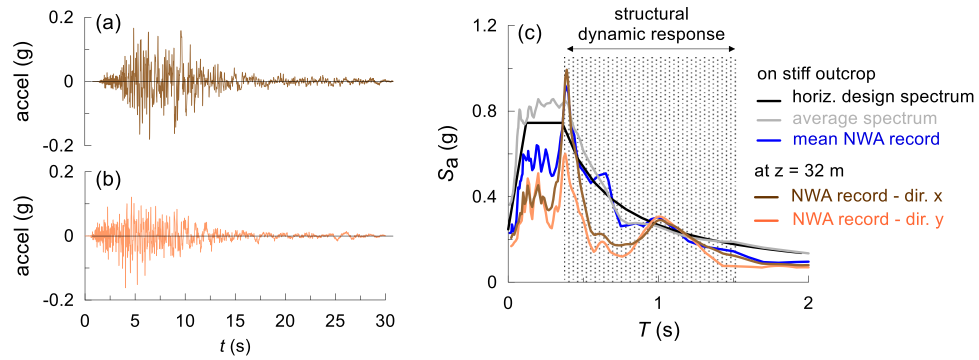

FIGURE 11 | (a, b) acceleration time histories of the convoluted motion of the Northridge Wonderland Ave. (NWA) in the *x* and *y* direction, respectively; (c) comparison between the design spectrum of the horizontal motion, the 5%-damped average response spectrum of the selected records on stiff outcrop, the average spectrum of the reference seismic record at the outcrop and the corresponding convoluted spectra (brown and orange lines) (reproduced from Gorini et al. [7]).

reflecting the typical features of Messina Gravels down to the lower boundary of the domain placed at 32 m of depth. The soil was discretised using SSPbrick-type hexahedral elements [43] with constitutive behaviour governed by the Pressure Dependent Multi-Yield (PDMY) model [44]. Under static conditions, the soil nodes along the lateral boundaries were restrained to move in the vertical direction only, whereas the base nodes were fully fixed. In the dynamic stage, the lateral restraints were replaced by kinematic constraints enforcing equal displacements between the boundary nodes on opposite sides at the same elevation.

The seismic input for the coupled soil-structure model was defined in accordance with the seismic hazard of the Messina site [41, 42]. Among the suite of spectrum-compatible ground motions selected in Gorini et al. [7], the 1994 Northridge WA earthquake record (Northridge Wonderland Ave., RSN 1011, https://ngawest2.berkeley.edu/) is taken as a reference for validating the SSI-informed design criterion. This record corresponds to a Life Safety Limit State seismic scenario for the building at hand (return period of 475 years). The acceleration time histories of the horizontal components of the record are shown in Figures 11a,b, and the associated 5%-damped elastic response spectra are compared against the Life-Safety design spectrum in Figure 11c.

We investigate the potential of TMDs with different configurations to attenuate earthquake-induced demands on the building. The TMD mass ratio G_1 ranges from 5% to 30%. For conventional devices ($G_1 = 5\%$), the TMD is located at the modal height of the building and modelled as a lumped mass connected to it through the parallel connection of a linear spring and a damper. The TMD mass can move relatively to the structure in the x-direction only. The TMD properties were determined following the well-known design procedure by Den Hartog [1]. For G_1>5%, the so-called Large-Mass ratio TMD (LM-TMD) was implemented by introducing additional masses atop each column at the top floor, proportioned to their tributary areas. This simplified technique facilitates the manageable update of the coupled numerical model by allowing for a straightforward modification of the TMD properties. The LM-TMD masses are connected to the main system via an assembly of elastomeric and flat slider bearings exhibiting elastic-plastic behaviour, as detailed in Gorini et al. [7]. Their mechanical properties were designed to match the target tuning frequency and damping ratio prescribed by the design method in Marrazzo et al. [15], which extends Den Hartog's formulation to larger mass ratios, albeit without accounting for soil-structure interaction.

5.2.2 | Seismic Performance of the SSI-Informed Design Criterion for TMDs on the Reference Seismic Scenario

The seismic response of the reference soil-building-TMD model subjected to both horizontal components of the selected ground motion is assessed by comparing two scenarios: one where the TMD is designed using the standard criteria introduced in Section 5.2.1, and another where the mechanical properties of the TMD are derived according to the proposed SSI-informed methodology. The seismic performance is summarised in Figure 12, which represents the Maximum Interstory Drift (MID) along an edge vertical alignment of the building (no significant discrepancies in MID are observed among different alignments), considering both the standard and SSI-informed design and varying the mass ratio. The MID is computed as the maximum relative horizontal displacement for each floor, divided by the floor height.

It is noteworthy that with the standard design (Figure 12a) a TMD having a relatively low mass ratio ($G_1 \leq 10\%$) even causes a significant increment of the MID at the sixth floor. This detrimental effect can be ascribed to two factors. First, at floor No. 6, where the column cross sections become smaller, a soft story mechanism is activated during the seismic event causing the MID to spike. This is a consequence of the non-seismic technical provisions used in the design of the existing building. As a result, the TMD becomes detuned from the target response assumed in design, failing to account for the nonlinear structural behaviour exhibited during the seismic event. Secondly, the calibration of the TMD's mechanical properties is based on the fundamental frequency of the building in the x-direction only, causing further detuning due to the multi-directionality of the seismic motion that excites multiple vibration modes in both horizontal directions. This was confirmed through additional analyses considering the soil-building-TMD model perturbed by the sole x-component of the seismic record, whose results are omitted for conciseness. The analyses revealed that a TMD tuned to the fundamental frequency of the superstructure in the direction of motion significantly

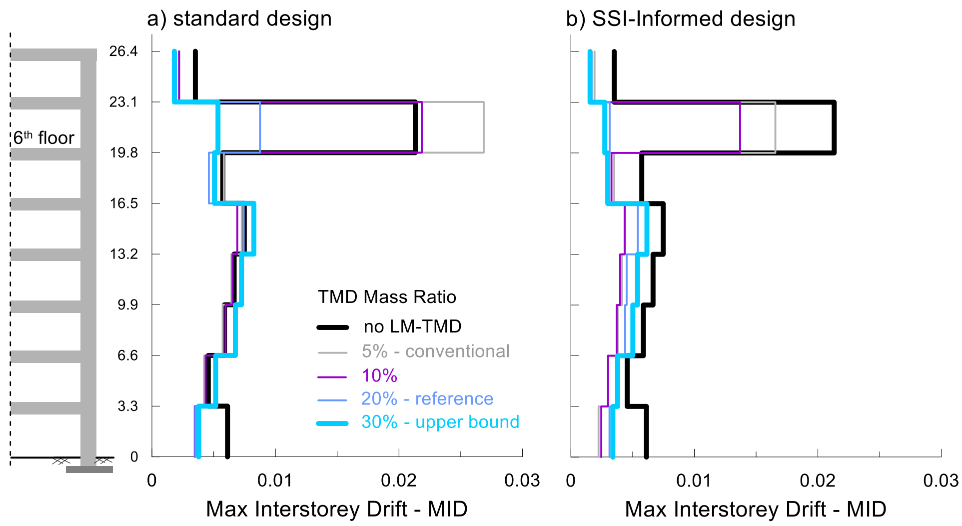

FIGURE 12 | Performance of the building subjected to both horizontal components of the reference ground motion: comparison between the maximum inter-story drifts in the horizontal direction considering the presence or not of the TMD, the latter designed (a) according to a standard criterion and (b) to the SSI-informed criterion, for different mass ratios.

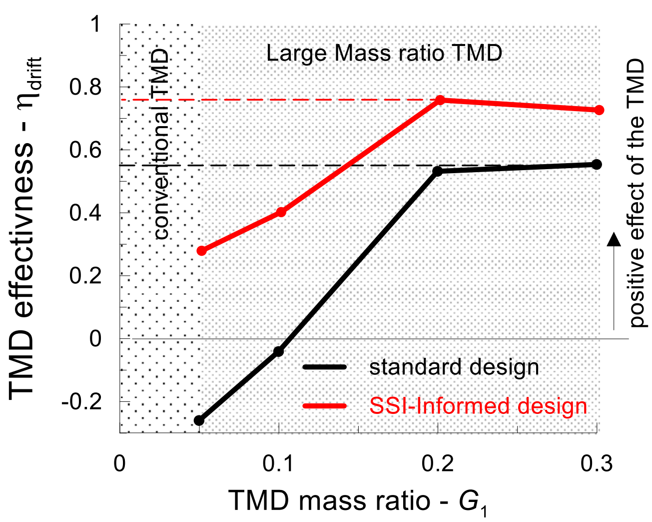

FIGURE 13 | Performance of the building subjected to both horizontal components of the reference ground motion: variability with the mass ratio *G*1 of the TMD effectiveness considering the standard and SSI-informed design.

reduces the drift demand, reaching an effectiveness of η = 40% and 55% for G_1 = 5% and 30% respectively. To mitigate the negative effects observed when considering both horizontal components of the ground motion, a sufficiently large mass ratio is required, with $G_1 \geq 20\%$ proving effective for the case under examination. In particular, a 30%-mass ratio avoids the soft story mechanism, at the cost of an increased drift demand on lower floors.

In contrast, the SSI-informed design (Fig. 12b) reduces the MID across all floors, especially at the sixth floor and the base columns. This enhanced performance is further illustrated in Figure 13 in terms of the TMD performance curve, representing the relationship between η and the TMD mass ratio. A key takeaway from the figure is that leveraging soil-structure interaction can substantially boost the seismic performance. For both standard and SSI-informed designs, the TMD effectiveness increases more than linearly with the mass ratio up to G_1 = 20%, whilst it stabilises for G_1>20%. This sort of saturation effect of the TMD effectiveness, already observed in Gorini et al. [7], can be attributed to a combination of factors relating to soil-structure interaction, such as the attainment of the soil strength and the increased dominance of the foundation rocking as the nonlinear behaviour of the foundation soils intensifies.

For the case study at hand, the SSI-informed criterion improves the structural performance (η>0) even for low TMD mass ratios. Interestingly, as the TMD mass ratio decreases the mitigation of structural vibration becomes more pronounced. In detail, the effectiveness of the SSI-informed TMD is equal to 29% for G_1 = 5%, instead of η = -26% obtained with the standard design, and peaks at 77% for large G_1, corresponding to a reduction of the drift demand of 39% compared to standard design.

On the basis of the validation process discussed so far, the SSI-informed design proves to be more robust than the standard design neglecting the interaction with the foundation soils. Indeed, an SSI-informed TMD i) prevents detrimental effects, especially at low mass ratios where the device is more vulnerable to soil-structure interaction, and ii) effectively controls inertial forces across a broader range of periods, including those relating to combined translational-rotational deformation modes of the entire soil-structure system, thereby limiting the adverse effects of multi-directional ground motion.

5.2.3 | Effect of the Record-to-Record Variability

The robustness of the proposed SSI-informed design is further assessed by accounting for the variability of the seismic input. To this end, the benchmark soil-structure-TMD system described in Section 5.2.1 was subjected to both horizontal components of two additional ground motions, the Loma Prieta and Northridge VRP records, compatible with the Life-Safety Limit State of the

TABLE 6 | Characteristics of the selected life-safety seismic records (mean period T_m provided for both horizontal components).

No.	Record	Event name	I_A (m/s)	T_s (s)	T_m (s)	$V_{s,30}$ (m/s)	M_w (-)	R_{JB} (km)
1	RSN 765	Loma prieta	1.7	11.4	0.33/0.49	1428	6.93	8.84
2	RSN 1011	Northridge, WONDERLAND Ave. (WA)	0.2	12.7	0.44/0.33	1223	6.69	15.11
3	RSN 1091	Northridge, Vasquez Rocks Park (VRP)	0.4	15.4	0.51/0.52	996	6.69	23.1

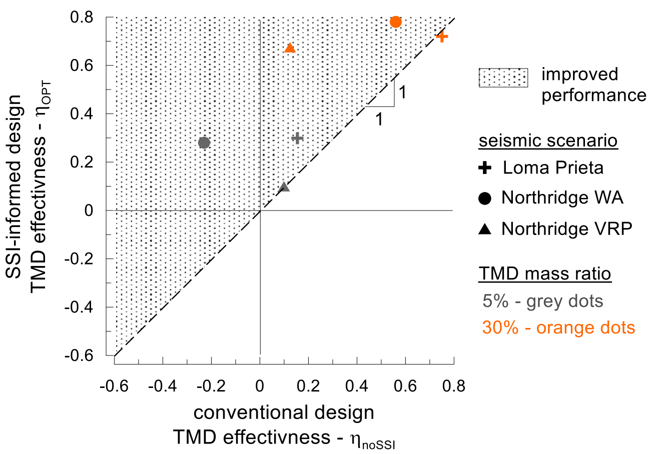

FIGURE 14 | Performance of the reference building subjected to both horizontal components of the considered, life-safety seismic scenarios: comparison between the TMD effectiveness obtained with the SSI-informed design and the conventional design, for mass ratios equal to 5% and 30%.

building. These records were selected from the same spectrum-compatible set adopted in Gorini et al. [7]. As testified by their main features listed in Table 6, the selected ground motions are representative of distinct frequency contents and time-domain characteristics, while preserving consistency with the seismic hazard of the Messina site. In the table, I_A is the Arias Intensity, T_s is the significant duration, T_m is the mean period of the seismic record [45], $V_{S,30}$ is the average shear wave velocity in the upper 30 m of depth, M_w is the moment magnitude and R_{JB} the Joyner and Boore distance.

For each seismic scenario, nonlinear dynamic analyses were performed considering the structure without and with the TMD. In the latter case, the boundary values assumed in Section 5.2.2 were adopted for the TMD mass ratio, namely $G_1 = 5\%$ and 30%.

Figure 14 compares the drift-based effectiveness of the TMD obtained with the SSI-informed design and with the conventional design approaches employed in Section 5.2.2, for the three seismic records considered. The results highlight a systematic improvement provided by the SSI-informed criterion, irrespective of the specific characteristics of the seismic input. For both mass ratios examined, the proposed design always yields a notable effectiveness, whereas the conventional design exhibits a marked sensitivity to the seismic excitation. This effect is particularly evident for $G_1 = 5\%$, in which the effectiveness drops significantly and becomes even negative for the Northridge WA record. This evidence confirms the remarkable detuning pointed out in Section 5.2.2, caused by (i) the pronounced nonlinear response of the foundation soils, (ii) the bidirectionality and broad frequency content of the seismic input, and (iii) the triggering of a soft story mechanism at floor No. 6. Notwithstanding, the SSI-informed design can manage their combined impact, leading to a remarkable reduction of earthquake-induced structural deformations. These beneficial effects are even amplified in those scenarios where soil-structure interaction is more pronounced.

5.2.4 | Efficacy of the SSI-Informed Design Under Varying Structure-to-Soil Relative Stiffness

The SSI-informed method is finally tested with respect to variations in the structure-to-soil relative stiffness, G_6. To this end, a modified version of the benchmark system described in Section 5.2.1 is developed. Specifically, the original eight-story RC building was reconceived as a six-story structure, while preserving the same plan dimensions, and the soil stiffness was varied by adopting $V_{s,30}$ = 180 m/s instead of 288 m/s of the original layout in Section 5.2.1 (according to European standards, this corresponds to soil category D instead of C of the initial layout). The structural members were redesigned accordingly, resulting in an increase of G_6 from 0.14, in the initial configuration, to 0.22, largely shifting the system towards the performance region in which soil-structure dynamic coupling is dominant [28].

For the modified configuration, nonlinear dynamic analyses were carried out considering the same Life-Safety seismic scenarios adopted in Section 5.2.3, with both horizontal components of the ground motion applied simultaneously. The investigation focused on the same TMD mass ratios, modelling assumptions and design approaches adopted therein, ensuring full consistency of the validation framework.

Figure 15 compares the drift-based effectiveness of the TMD obtained with the SSI-informed design and with the conventional design for the modified soil-structure system. The results confirm that increasing the structure-to-soil relative stiffness exacerbates the detuning effects observed for the conventional design, particularly for the low mass ratio configuration.

In contrast, the SSI-informed design consistently improves the effectiveness across all seismic inputs and for both mass ratios considered. This demonstrates the capability of the proposed criterion to adapt the TMD tuning to changes in the dynamic

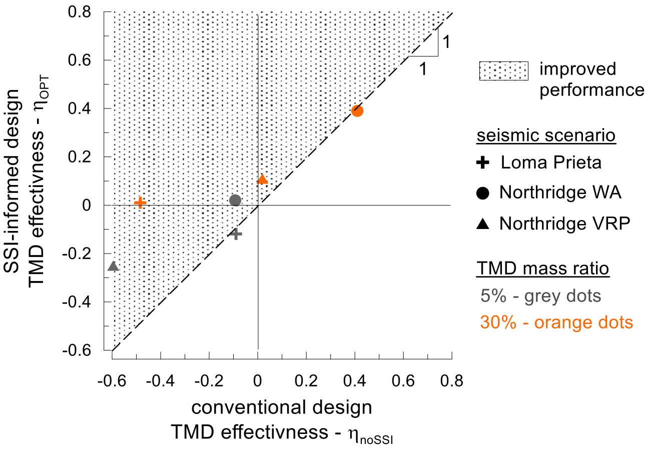

FIGURE 15 | Performance of the modified, six-story soil-building system subjected to both horizontal components of three Life-Safety seismic scenarios: comparison between the TMD effectiveness obtained with the SSI-informed design and the conventional design, for mass ratios equal to 5% and 30%.

coupling between the structure and the foundation system, effectively controlling the combined translational-rotational deformation modes that become increasingly relevant as G_6 rises. A decisive increase in the TMD effectiveness is observed even in scenarios where the standard design produces strongly detrimental effects ($\eta_{\mathrm{noSSI}}<0$).

Only in two cases the SSI-informed criterion does not fully convert highly unfavourable SSI conditions, manifesting on the TMD performance when using conventional design, into a superior tuning of the device, namely for G_1 = 5% under the Loma Prieta and Northridge VRP scenarios. This behaviour is attributed to the concurrent presence of several adverse factors, emphasised by the impulsive nature of these records, that are the bidirectionality and broad frequency content of the seismic input, the pronounced nonlinear soil response and the activation of plastic story mechanisms. These detrimental effects could be largely mitigated by equipping the structure with an additional TMD working in the orthogonal horizontal direction (see the discussion on seismic bidirectionality in Section 5.2.3) and, to a lesser extent, by explicitly incorporating nonlinear soil behaviour within the SimilSDOF interpretative model. Notwithstanding the simplifications introduced in the current formulation, the SSI-informed design still provides a marked improvement in performance with respect to the conventional approach, precisely by managing conveniently the same interaction mechanisms that undermine standard tuning strategies.

6 | Conclusions

This study has shown that soil-structure interaction is not merely a complicating factor to be considered in seismic design but can be leveraged as an opportunity to enhance hazard protection of buildings. The inherent dynamics of soil-structure systems can be strategically exploited to modulate the dynamic response and enable a more efficient management of the trade-off between inertia forces and energy dissipation across the entire system. Indeed, the interaction of a structure with the surrounding soil can worsen the performance, but it also opens the door to performance enhancements that are otherwise inaccessible in conventional design neglecting the soil compliance. These optimal configurations were found to depend on a limited set of nondimensional parameters governing the TMD behaviour, most notably, the structure-to-soil relative stiffness and parameters relating to the distribution of mass in the structural layout, which influence the contribution of foundation rocking.

Using this nondimensional framework in conjunction of a low-order interpretative model, a solution for the optimal resonance frequency of TMDs was devised. The solution was obtained via a multi-dimensional best fitting algorithm that links the TMD tuning factor to the dominant parameters describing the soil-structure layout. The resulting design law proved capable of identifying the TMD resonance frequency with reasonable accuracy across the entire seven-dimensional space of the dominant parameters, yielding a global coefficient of determination R^2 = 0.75 and a maximum local deviation of 16% for G_1 = 10% and 6% for G_1>10%, over the full dataset of 373’248 soil-structure-TMD cases.

In a complementary manner, the damping ratio G_3 of the TMD can be selected based on the mass ratio G_1: for G_1>20%, higher G_3 yield improved performance; for G_1≤20%, this proportionality no longer holds, and existing optimised solutions for G_3 (neglecting soil-structure interaction) can be used, as the optimised performance becomes primarily controlled by the tuning factor. Thus, within the nondimensional framework of the SimilSDOF adopted as a practice-oriented interpretative basis for dynamic soil-structure-TMD interactions, the SSI-informed design approach is applicable to devices with both low and large mass ratios, directly providing optimised TMD properties without the need for iterative numerical analyses or exhaustive implementations. It relies on a rigorous non-dimensional formulation, ensuring applicability across diverse structural configurations and subsoil conditions.

The proposed SSI-informed design was validated according to a two-stage process. First, the analytical optimised criterion was confirmed to reliably reproduce numerical results across a comprehensive set of soil-structure-TMD layouts. Then, the criterion was applied to design a TMD for a well-documented case study of a reinforced concrete building with subsoil conditions representative of the Messina Strait (South of Italy). By carrying out a parametric study on coupled soil-structure models, it was demonstrated the effectiveness of the optimised TMD in i) enhancing remarkably structural performance and ii) avoiding detrimental effects induced by soil-structure interaction. The SSI-informed criterion proved capable of mitigating unfavourable phenomena associated with nonlinear soil behaviour, such as the lengthening of resonance periods, the coupling of translational and rotational deformation modes and the exacerbation of irreversible effects. This performance stems from its intrinsic foundation on the governing parameters of soil-structure-TMD dynamics. For the reference benchmark, the proposed design increased the TMD effectiveness by up to 55% and 21% compared to the conventional design, for low and large mass ratios respectively. Moreover, the benefits of the proposed design were shown to be robust with respect to both record-to-record variability and variations in the structure-to-soil relative stiffness.

This work represents a step towards SSI-integrated seismic protection strategies. The present formulation is developed for dry soil conditions and does not explicitly address hydro-mechanical coupling or liquefaction phenomena. Extending the SSI-informed framework to saturated and potentially liquefiable soils represents a natural development of the method, together with the inclusion of nonlinear soil behaviour, alternative control devices and diverse structural typologies.

Acknowledgments

Open access publishing facilitated by Universita degli Studi di Trento, as part of the Wiley - CRUI-CARE agreement.

Conflicts of Interest

The authors declare no conflicts of interest.

Data Availability Statement

Data available on request from the authors.

References

1. J. P. Den Hartog, *Mechanical Vibrations* (Mc-Graw Hill, 1956).

2. J. Salvi, E. Rizzi, E. Rustighi, and N. S. Ferguson, "Optimum Tuning of Passive Tuned Mass Dampers for the Mitigation of Pulse-Like Responses," *Journal of Vibration and Acoustics, Transactions of the ASME* 140, no. 6 (2018): 061014, https://doi.org/10.1115/1.4040475.

3. O. Lavan, "Multi-Objective Optimal Design of Tuned Mass Dampers," *Structural Control and Heal Monitoring* 24, no. 11 (2017): 1–16, https://doi.org/10.1002/stc.2008.

4. D. Du, X. J. Gu, D. Y. Chu, and H. Hua, "Performance and Parametric Study of Infinite-Multiple TMDs for Structures Under Ground Acceleration by H∞ Optimization," *Journal of Sound and Vibration* 305, no. 4–5 (2007): 843–853, https://doi.org/10.1016/J.JSV.2007.05.003.

5. R. Rana and T. T. Soong, "Parametric Study and Simplified Design of Tuned Mass Dampers," *Engineering Structures* 20, no. 3 (1998): 193–204, https://doi.org/10.1016/S0141-0296(97)00078-3.

6. D. N. Gorini and C. Chisari, "Effect of Soil-Structure Interaction on Seismic Performance of Tuned Mass Dampers in buildings," in Earthquake Geotechnical Engineering for Protection and Development of Environment and Constructions. In *Proceedings of the 7th International Conference on Earthquake Geotechnical Engineering*, May 2020, International Society for Soil Mechanics and Geotechnical Engineering (CRC Press, 2019), 2690–2697, https://doi.org/10.1201/9780429031274.

7. D. N. Gorini, P. R. Marrazzo, E. Nastri, and R. Montuori, "Effectiveness of an Innovative Seismic Resilient Superelevation in an Archetype, Existing Soil-Structure System," *Bulletin of Earthquake Engineering* 23 (2025): 1677–1705, https://doi.org/10.1007/s10518-024-02050-4.

8. G. B. Warburton, "Optimum Absorber Parameters for Various Combinations of Response and Excitation Parameters," *Earthquake Engineering & Structural Dynamics* 10, no. 3 (1982): 381–401, https://doi.org/10.1002/eqe.4290100304.

9. F. Sadek, B. Mohraz, A. W. Taylor, and R. M. Chung, "A Method of Estimating the Parameters of Tuned Mass Dampers for Seismic Applications," *Earthquake Engineering & Structural Dynamics* 26 (1997): 617–635, https://doi.org/10.1093/biomet/37.1-2.173.

10. R. S. Jangid and T. K. Datta, "Performance of Multiple Tuned Mass Dampers for Torsionally Coupled System," *Earthquake Engineering & Structural Dynamics* 26, no. 3 (1997): 307–317, https://doi.org/10.1002/(SICI)1096-9845(199703)26:3⟨307::AID-EQE639⟩3.0.CO;2-8.

11. L. Zuo and S. A. Nayfeh, "Optimization of the Individual Stiffness and Damping Parameters in Multiple-Tuned-Mass-Damper Systems," *Journal of Vibration and Acoustics, Transactions of the ASME* 127, no. 1 (2005): 77–83, https://doi.org/10.1115/1.1855929.

12. L. Wang, Y. Zhou, and Z. Zhou, "Seismic Response Control of tall Building Using Semi-Active Tuned Mass Damper Considering Soil-Structure Interaction," *Soil Dynamics and Earthquake Engineering* 187, no. 108987 (2024): 108987.

13. M. De Angelis, S. Perno, and A. Reggio, "Dynamic Response and Optimal Design of Structures With Large Mass Ratio TMD," *Earthquake Engineering & Structural Dynamics* 41 (2012): 41–60, https://doi.org/10.1002/eqe.1117.

14. M. Yahyai, L. Zebarjad, M. Head, and M. Shokouhian, "Optimum Parameters for Large Mass Ratio TMDs Using Frequency Response Function," *Journal of Earthquake Engineering* 25, no. 10 (2021): 2127–2146, https://doi.org/10.1080/13632469.2019.1624228.

15. P. R. Marrazzo, R. Montuori, E. Nastri, and G. Benzoni, "Advanced Seismic Retrofitting With High-Mass-Ratio Tuned Mass Dampers," *Soil Dynamics and Earthquake Engineering* 179, no. 958 (2024): 108544, https://doi.org/10.1016/j.soildyn.2024.108544.

16. M. C. Smith, "Synthesis of Mechanical Networks: The Inerter," *IEEE Transactions on Automatic Control* 47, no. 10 (2002): 1648–1662, https://doi.org/10.1109/TAC.2002.803532.

17. M. Z. Q. Chen, Y. Hu, L. Huang, and G. Chen, "Influence of Inerter on Natural Frequencies of Vibration Systems," *Journal of Sound and Vibration* 333, no. 7 (2014): 1874–1887, https://doi.org/10.1016/j.jsv.2013.11.025.

18. W. Shen, A. Niyitangamahoro, Z. Feng, and H. Zhu, "Tuned Inerter Dampers for Civil Structures Subjected to Earthquake Ground Motions: Optimum Design and Seismic Performance," *Engineering Structures* 198 (2019): 109470, https://doi.org/10.1016/j.engstruct.2019.109470.

19. F. Qian, Y. Luo, H. Sun, W. C. Tai, and L. Zuo, "Optimal Tuned Inerter Dampers for Performance Enhancement of Vibration Isolation," *Engineering Structures* 198 (2019): 109464, https://doi.org/10.1016/j.engstruct.2019.109464.

20. S. Elias and S. Djerouni, "Optimum Tuned Mass Damper Inerter Under Near-Fault Pulse-Like Ground Motions of Buildings Including Soil-structure Interaction," *Journal of Building Engineering* 85 (2024): 108674.

21. O. Araz and E. N. Farsangi, "Optimum Tuned Tandem Mass Dampers for Suppressing Seismic-Induced Vibrations Considering Soil-Structure Interaction," *Structures* 52 (2023): 1146–1159, https://doi.org/10.1016/j.istruc.2023.04.017.

22. O. Araz, S. Elias, and F. Kablan, "Seismic-Induced Vibration Control of a Multi-Story Building With Double Tuned Mass Dampers Considering Soil-Structure Interaction," *Soil Dynamics and Earthquake Engineering* 166 (2023): 107765, https://doi.org/10.1016/j.soildyn.2023.107765.

23. O. Araz, M. Kazemi, and S. Elias, "Effect of Basic Parameters Defining Principal Soil-Structure Interaction on Seismic Control of Structures Equipped With Optimum Tuned Mass Damper," *Soil Dynamics and Earthquake Engineering* 190 (2025): 109041.

24. J. Wu, G. Chen, and M. Lou, "Seismic Effectiveness of Tuned Mass Dampers Considering Soil-Structure Interaction," *Earthquake Engineering & Structural Dynamics* 28, no. 11 (1999): 1219–1233, https://doi.org/10.1002/(SICI)1096-9845(199911)28:11⟨1219::AID-EQE861⟩3.0.CO;2-G.

25. I. Takewaki, "Soil-Structure Random Response Reduction via TMD-VD Simultaneous Use," *Computer Methods in Applied Mechanics and Engineering* 190, no. 5–7 (2000): 677–690.

26. J. Wu, G. Chen, and M. Lou, "Seismic Effectiveness of Tuned Mass Dampers Considering Soil-Structure Interaction," *Earthq Eng Struct Dyn* 28, no. 11 (1999): 1219–1233.

27. A. Ghosh and B. Basu, “Effect of Soil Interaction on the Performance of Tuned Mass Dampers for Seismic Applications,” *Journal of Sound and Vibration* 274, no. 3–5 (2004): 1079–1090.

28. D. N. Gorini and C. Chisari, “Impact of Soil-structure Interaction on the Effectiveness of Tuned Mass Dampers,” *Earthquake Engineering & Structural Dynamics* 51, no. 6 (2022): 1501–1521, https://doi.org/10.1002/eqe.3625.

29. A. Farshidianfar and S. Soheili, “Ant Colony Optimization of Tuned Mass Dampers for Earthquake Oscillations of High-Rise Structures Including Soil-Structure Interaction,” *Soil Dynamics and Earthquake Engineering* 51, no. 1 (2013): 14–22.

30. A. Farshidianfar and S. Soheili, “ABC Optimization of TMD Parameters for tall Buildings With Soil Structure Interaction,” *Interactions and Multiscale Mechanics* 6, no. 4 (2013): 339–356.

31. G. Bekdaş and S. M. Nigdeli, “Metaheuristic Based Optimization of Tuned Mass Dampers Under Earthquake Excitation by Considering Soil-Structure Interaction,” *Soil Dynamics and Earthquake Engineering* 92 (2017): 443–461, https://doi.org/10.1016/j.soildyn.2016.10.019.

32. J. Salvi, F. Pioldi, and E. Rizzi, “Optimum Tuned Mass Dampers Under Seismic Soil-Structure Interaction,” *Soil Dynamics and Earthquake Engineering* 114, no. 4 (2018): 576–597, https://doi.org/10.1016/j.soildyn.2018.07.014.

33. S. Dassault, *ABAQUS 6.12-I Documentation*, Published online (Dassault Systémes, 2013).

34. F. McKenna, M. H. Scott, and G. L. Fenves, “OpenSees. Nonlinear Finite-Element Analysis Software Architecture Using Object Composition,” *Journal of Computing in Civil Engineering* 24 (2010): 95–107.

35. G. Gazetas, “Foundation Vibrations,” in *Foundation Engineering Handbook* (Springer, 1991), 553–593, https://doi.org/10.1007/978-1-4615-3928-5_15.

36. MATLAB, “The MathWorks Inc”.

37. M. Morris, “Factorial Sampling Plans for Preliminary Computational Experiments,” *Technometrics* 33, no. 2 (1991): 161–174.

38. Decreto Ministeriale 16 giugno, “Norme Tecniche per la Esecuzione Delle Opere in Cemento Armato Normale e Precompresso e per le Strutture Metalliche,” 1976.

39. F. Taucer, E. Spacone, and F. C. Filippou, “A Fiber Beam-Column Element for Seismic Response Analysis of Reinforced Concrete Structures,” 1991, *Report No. UCB/EERC-91/17*.

40. A. Neuenhofer and F. C. Filippou, “Geometrically Nonlinear Flexibility-Based Frame Finite Element,” *Journal of Structural Engineering* 124, no. 6 (1998): 704–711.

41. D. N. Gorini, *Soil-Structure Interaction for Bridge Abutments : Two Complementary Macro-Elements* (Sapienza University of Rome, 2019), https://iris.uniroma1.it/handle/11573/1260972.

42. D. N. Gorini and L. Callisto, “A Coupled Study of Soil-Abutment-Superstructure Interaction,” in Lecture Notes in Civil Engineering. “Geotechnical Research for Land Protection and Development”, *Proceedings of CNRIG2019*, Italian Geotechnical Association (Springer, 2019), 565–574, https://doi.org/10.1007/978-3-030-21359-6_60.

43. O. C. Zienkiewicz and T. Shiomi, “Dynamic Behaviour of Saturated Porous Media; the Generalized Biot Formulation and Its Numerical Solution,” *International Journal for Numerical and Analytical Methods in Geomechanics* 8, no. 1 (1984): 71–96.

44. Z. Yang, A. Elgamal, and E. Parra, “Computational Model for Cyclic Mobility and Associated Shear Deformation,” *Journal of Geotechnical and Geoenvironmental Engineering* 129, no. 12 (2003): 1119–1127, https://doi.org/10.1061/(asce)1090-0241(2003)129:12(1119).

45. E. M. Rathje, N. A. Abrahamson, and J. D. Bray, “Simplified Frequency Content Estimates of Earthquake Ground Motions,” *Journal of Geotechnical and Geoenvironmental Engineering* 124, no. 2 (1998): 150–159.

Appendix A

Figures A1, A2 complement the representation provided in Figure 3, illustrating the cases with $G_9 = 0.5$ and 0.75, respectively. Likewise, Figures A3, A4 extend the visualization presented in Figure 5.

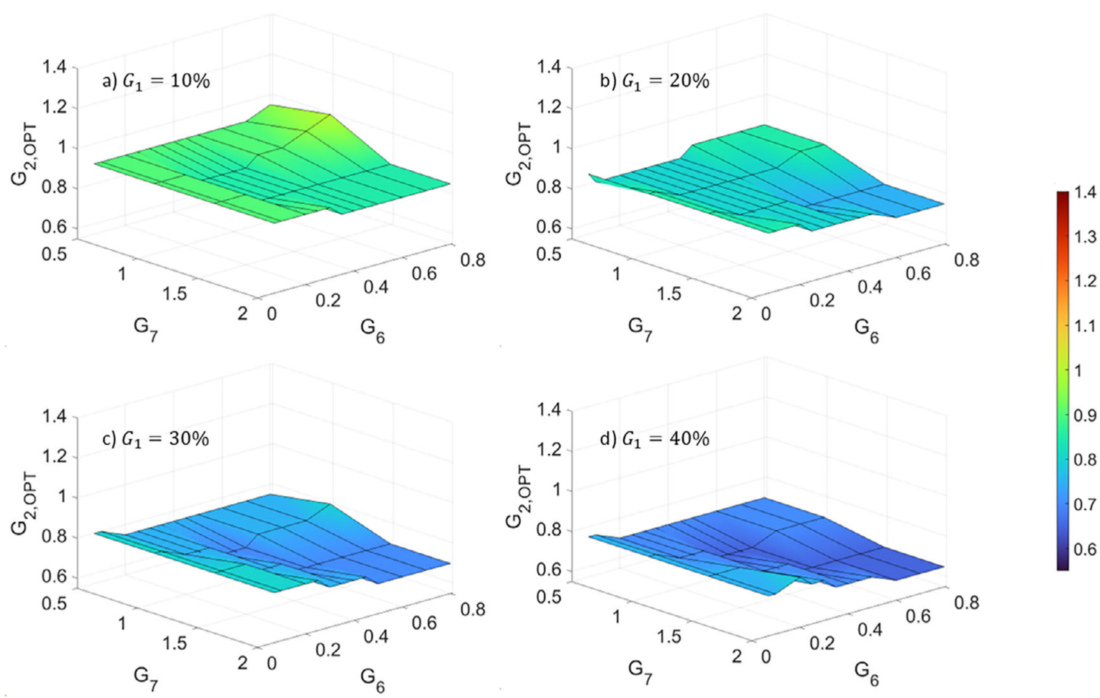

FIGURE A1 | Optimum values of the TMD frequency ratio, $G_{2,\mathrm{opt}}$, as a function of the structure-to-soil relative stiffness, G_6, and the structure slenderness ratio, G_7, for TMD mass ratios MR = 5,10,20,30% (a, b, c and d, respectively), for $G_9 = 0.5$.

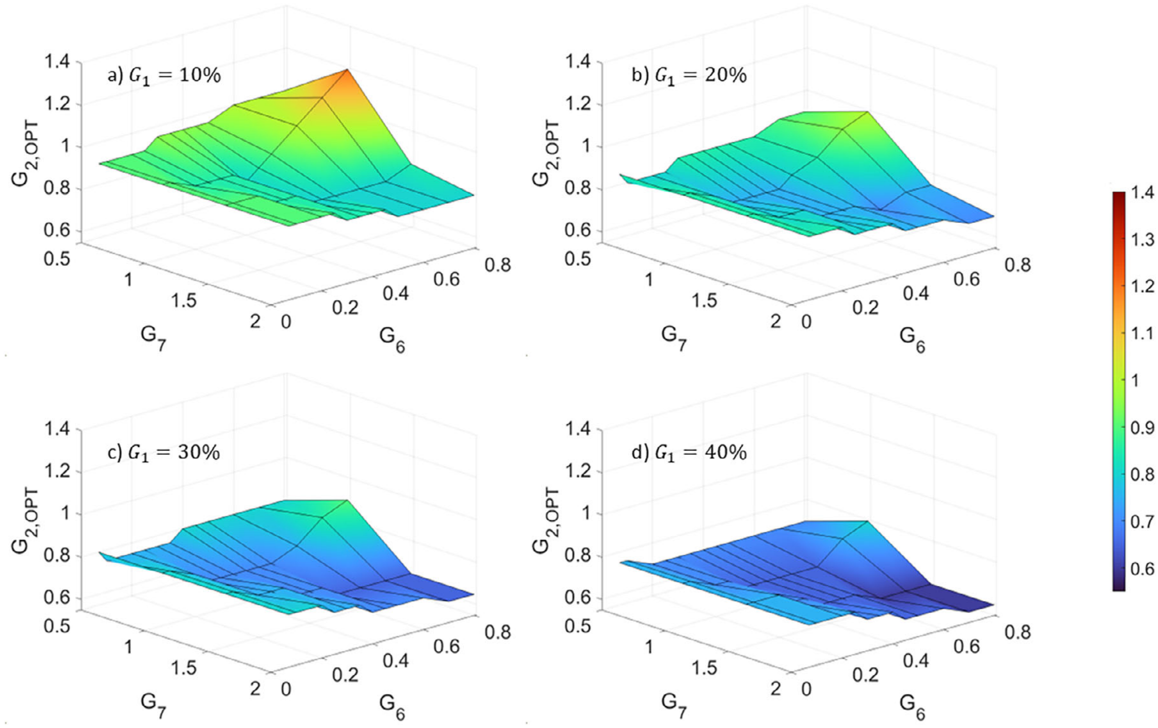

FIGURE A2 | Optimum values of the TMD frequency ratio, $G_{2,opt}$, as a function of the structure-to-soil relative stiffness, G_6, and the structure slenderness ratio, G_7, for TMD mass ratios MR = 5,10,20,30% (a, b, c and d, respectively), for $G_9 = 0.75$.

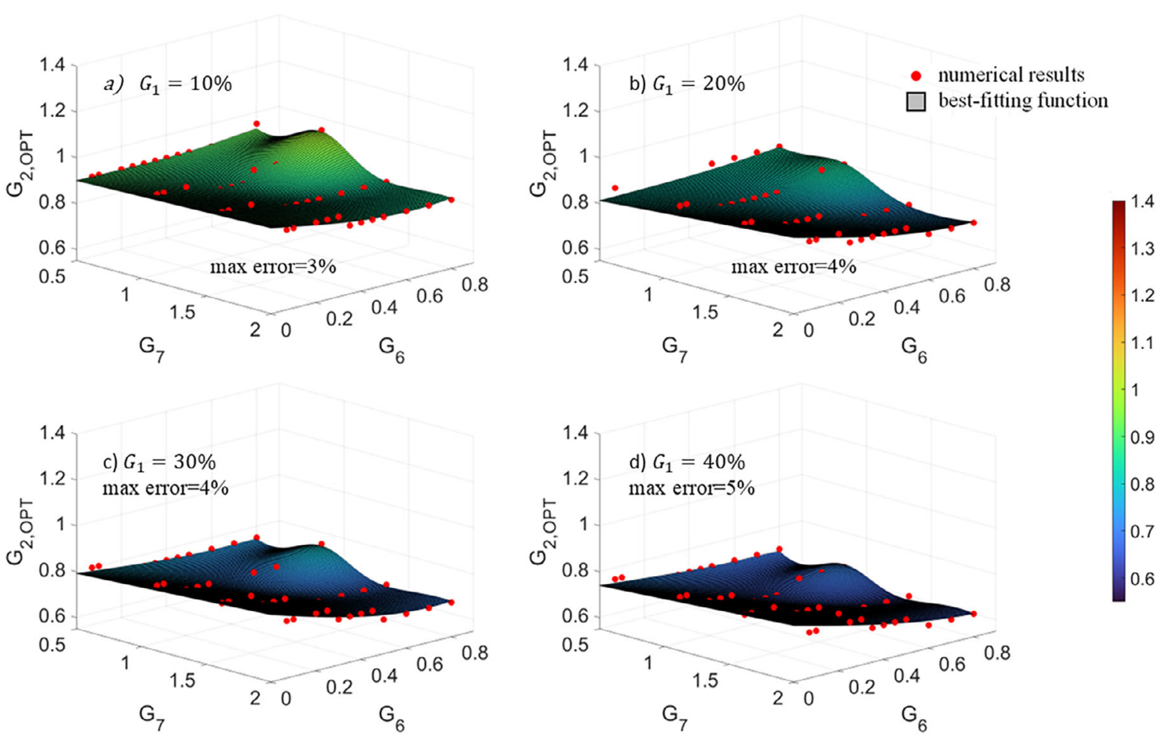

FIGURE A3 | Best-fitting function for the optimum TMD frequency ratio, $G_{2,opt}$, versus the SimilSDOF numerical results (dotted points) as a function of the structure-to-soil relative stiffness, G_6, and the structure slenderness ratio, G_7, for TMD mass ratios MR = 5,10,20,30% (a, b, c and d, respectively), for $G_9 = 0.5$.

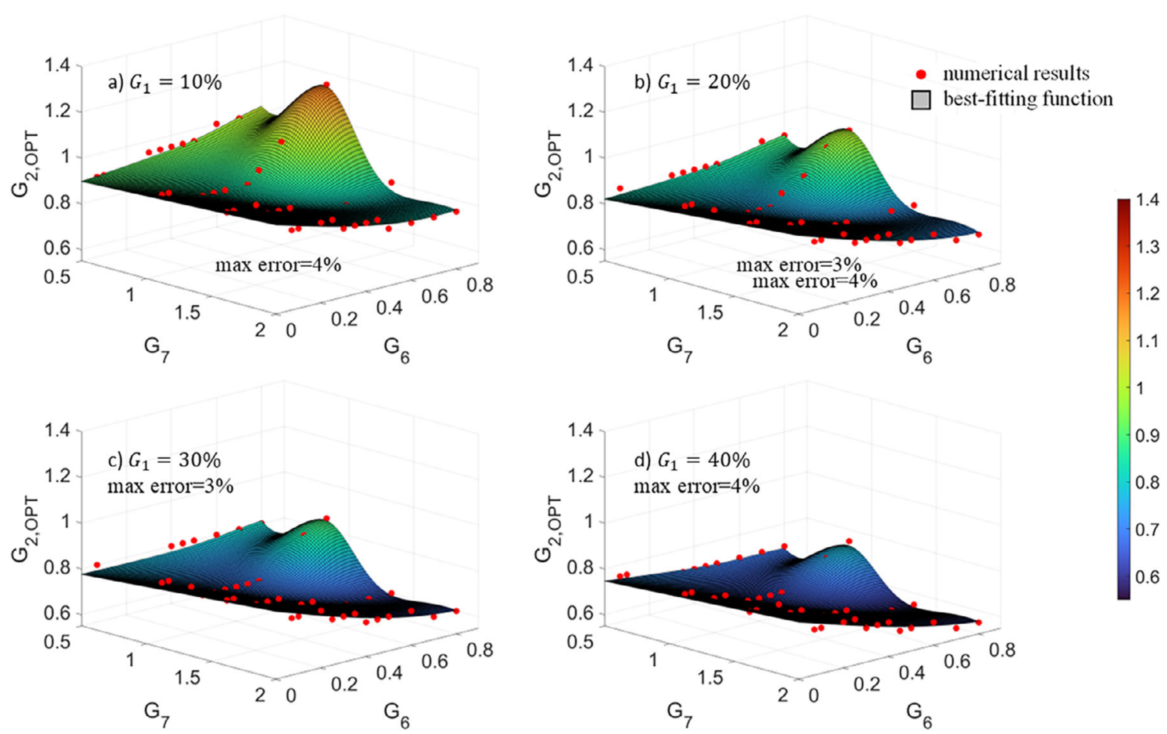

FIGURE A4 | Best-fitting function for the optimum TMD frequency ratio, $G_{2,opt}$, versus the SimilSDOF numerical results (dotted points) as a function of the structure-to-soil relative stiffness, G_6, and the structure slenderness ratio, G_7, for TMD mass ratios MR = 5,10,20,30% (a, b, c and d, respectively), for $G_9 = 0.75$.